Copyright © 1995, by the author(s).
All rights reserved.

Permission to make digital or hard copies of all or part of this work for personal or classroom use is granted without fee provided that copies are not made or distributed for profit or commercial advantage and that copies bear this notice and the full citation on the first page. To copy otherwise, to republish, to post on servers or to redistribute to lists, requires prior specific permission.

MODELING ELECTRONEGATIVE DISCHARGES AT LOW PRESSURE

by

I. Kouznetsov, A. J. Lichtenberg, and M. A. Lieberman

Memorandum No. UCB/ERL M95/97

29 November 1995

MODELING ELECTRONEGATIVE DISCHARGES AT LOW PRESSURE

by

I. Kouznetsov, A. J. Lichtenberg, and M. A. Lieberman

Memorandum No. UCB/ERL M95/97

29 November 1995

ELECTRONICS RESEARCH LABORATORY

College of Engineering
University of California, Berkeley
94720

MODELING ELECTRONEGATIVE DISCHARGES AT LOW PRESSURE

by

I. Kouznetsov, A. J. Lichtenberg, and *M. A. Lieberman*
Department of Electrical Engineering and Computer Sciences
and the Electronics Research Laboratory
University of California, Berkeley, CA 94720

Abstract

In a previous study, a macroscopic analytic model was developed for a plasma discharge with a three component (electronegative) core and an electropositive edge region. Both regions were treated in the high pressure approximation of constant mobility for the positive ions. We extend the treatment to low pressures, for which the ion thermal velocity within the electropositive region is much less than the ion flow velocity, by using a variable mobility model with constant mean free path for the positive ions. The density at the interface between the electropositive region and the sheath is determined by generalizing a low pressure electropositive solution to a finite flow boundary condition at the interface with the electronegative plasma. The results are also extended to include an additional transition region in which the flow within the electronegative region is not allowed to exceed the local ion sound speed, which can result in an abrupt decrease in negative ion density. The approximation of a parabolic negative ion profile results in algebraic equations which are solved numerically over a range of parameters. Typical cases are compared to particle-in-cell (PIC) Monte Carlo simulations.

I. Introduction

Plasma processing involves electronegative gases and gas mixtures. The number of equations governing the equilibrium is large and analysis becomes complicated. At the same time there is an increased need to understand the scaling of the plasma constituents with control parameters, since the parameter space is much enlarged from that of electropositive plasmas. In an early study of an electronegative positive column the continuity and force equations for a three species plasma, consisting of electrons, one positive ion, and one negative ion species, were solved numerically to obtain the equilibrium for a positive column [1]. However, the numerical results give little insight into the importance of various terms in the equations, and the scaling with parameters. Recent work has attempted to analyze such plasmas, using various simplifications to make the studies tractable [2–5]. In [2], the equilibrium equations were reduced to a coupled pair of nonlinear differential equations that were solved numerically, with some simplifying assumptions. In that work, as in [1] the positive column was treated as a single region, which therefore did not distinguish between the central electronegative core and the electropositive edge region. A simplified set of equations has also been used to solve qualitatively for the plasma parameters of a negative ion source [3]. In an alternative approach the two region nature of the problem was essentially recognized [4]. Various assumptions were used to uncouple the differential equations and reduce them to solvable form. In particular, recombination was neglected in favor of detachment which, together with other approximations, limit the applicability of the model [4].

In a previous study we developed a theory to treat an electronegative plasma in a parallel plane discharge when only a single positive ion species is important [5]. This was applied to a large aspect ratio cylindrical oxygen discharge (length $\ll$ diameter) at relatively low

density and relatively high pressure, in which dissociation of O_2 is not important. We also made the assumption that the Boltzmann relation holds for both negative species, electrons and O^-, such that a single ambipolar diffusion equation can be constructed to describe the equilibrium. The resulting ambipolar diffusion equation, including the recombination, is nonlinear, so that analytic solutions can not be obtained. However, it was shown that simpler approximate solutions are still possible if the plasma is divided into a core electronegative region and an edge electropositive region, each with a constant (but different) ambipolar diffusion coefficient. The resulting solutions were compared to particle-in-cell (PIC) Monte Carlo simulations, investigating the various approximations involved in the model development, and showing that they were generally justified. As in the various analyses of the positive column, the analysis was developed for a relatively high pressure regime for which constant diffusion and mobility, for each species, is a reasonable approximation [5].

In many electronegative plasmas more than one positive or negative ion species may be important. The work in [2] was generalized to include more species, but at the expense of obtaining a large set of coupled differential equations that could only be solved numerically [6]. A similar approach was used to obtain the equilibrium of a parallel plane discharge, also obtaining a set of coupled differential equations [7]. In another approach to the multi-species problem, we have developed a global, two-dimensional cylindrical model [8]. The model is particularly useful in high plasma density (high power) low pressure discharges, as in electron cyclotron resonance (ECR) and RF inductive sources, for which the electronegativity tends to be weak. The global model does not describe the spatial distribution of negative ions, but should preserve the essential scalings of plasma parameters with control parameters. The model also allowed the investigation of various phenomena, such as the

effects of excited species, by setting the corresponding reaction rates to zero, which gives us the information required to obtain the most relevant reduced set of species and reactions.

The purpose of this paper is to extend our previous work on a three species spatially varying plasma [5] to lower pressures for which a constant ion mobility model is not adequate to treat the electropositive edge region. Instead, a low pressure constant mean-free-path model [9] is used and generalized to include ion flow from a core electronegative region. The electronegative plasma core is also generalized to include an ion sound velocity limitation, and the electropositive region is allowed to vanish in some parameter ranges. Such a complex model does not have completely analytic equilibrium solutions. However, the assumption of a profile in the electronegative region, as in Ref. [5], reduces the problem to a set of coupled algebraic equations from which rather straightforward analytical and numerical results can be obtained. Examination of various limiting cases connects the results to our previous work [5] and exposes some of the important scalings. For the specific case of oxygen feedstock gas, the results of a global model [8] are used to guide the choice of the dominant reaction rates.

The structure of our model is illustrated in Fig. 1. The plasma is generally divided into two regions, an electronegative core and an electropositive edge, with a plane-parallel model considering only half of the plasma by symmetry. There is also a sheath between the plasma and an external wall or electrode, but we do not consider the details of this region within an equilibrium model. In Fig. 1a we sketch the density profile (solid lines) and a piecewise-constant-parameter approximation to it (dashed lines) when the ion sound speed does not limit the positive ion flow in the electronegative core. The core plasma consists primarily of positive ions and negative ions, with a smaller component of electrons. The density decreases from the center, with an approximate ambipolar diffusion equation governing

the positive ion diffusion. Assuming that the electrons and negative ions are in Boltzmann equilibrium with the electric fields, both negative species see containing fields, but the much more energetic electrons are only weakly affected, maintaining a nearly constant density, while the negative ion density follows the fall-off of the positive ion density. In a transition region in which the negative ion density is comparable to the electron density, the electric field increases, reducing the negative ion density to small values, where the plasma becomes essentially electropositive. This transition region is generally thin such that it is reasonable to approximate the transition as abrupt. In the electropositive region an ambipolar diffusion solution applies in which the electric fields contain the energetic electrons. The density decreases to a value n_s and the flux increases such that the Bohm velocity $u_{B0} = (eT_e/M)^{1/2}$ is reached at the transition to the sheath. To obtain simple algebraic equations for the equilibrium, we use approximate profiles in both the electronegative and electropositive regions. As we shall show in the following sections, a parabolic negative ion profile is a good approximation for the electronegative region. We obtain an exact solution for the positive ion profile in the electropositive region at low pressures; however a uniform density which drops abruptly to an edge density n_s at the sheath is usually an adequate approximation.

In Fig. 1b we show similar profiles in a parameter regime in which the positive ion diffusion velocity u_+ reaches the local ion sound speed u_B within the electronegative core. Here u_B is less than u_{B0} due to the presence of the negative ions. In this case we expect a space charge region to form [10] which, in some aspects, is similar to a sheath that forms at a wall. An electric field that builds up in this region leads to the rapid fall of the negative ion density, over a few electron Debye lengths, and the positive ion density approaches the weakly varying electron density, until an electropositive plasma with $u_+ < u_{B0}$ is formed. The electropositive plasma has the same form as in Fig. 1a. An approximate solution for

the negative ion density profile in the electronegative core is then a section of a parabola with an abrupt density drop to the electropositive edge.

In Section II we obtain the generalized low pressure solution for the electropositive edge plasma including the flow from the electronegative core. In Section III we review the electronegative assumptions and generalize the results to include an ion sound limitation. The density and flux at the boundary between the two regions are matched to complete the model. In Section IV various approximations are developed to expose the dominant scalings and to obtain simpler solutions. In Section V we apply the approximate solutions to the case of an oxygen plasma. For specific values we compare the results to PIC simulations [11] as has also been done in [5]. We leave the extension of the analysis to more positive ion species to a future paper.

II. Low Pressure Solution in the Electropositive Region

When the electron temperature is much larger than the ion temperature, a common situation in discharges, the ion and the electron motion can be described by the ambipolar diffusion equations, consisting of an approximate electric field driven flux equation for ions,

$$\mathbf{\Gamma}_+ = \mu_+ n_+ \mathbf{E}, \tag{2.1}$$

a Boltzmann equilibrium for electrons,

$$n_e = n_{e0} \exp\left(\frac{\Phi}{T_e}\right), \tag{2.2}$$

and the positive ion conservation relation

$$\nabla \cdot \mathbf{\Gamma}_+ = \nu_{iz} n_+. \tag{2.3}$$

Here μ_+ is the ion mobility, $\nu_{iz} = K_{iz} n_0$ is the ionization rate, K_{iz} is the ionization rate constant, n_0 is the neutral gas density, n_{e0} is the electron concentration at the boundary

with the electronegative region, and $\mathbf{E} = -\nabla\Phi$ is the electric field. The charge neutrality in the bulk requires $n_e = n_+ = n$.

At lower pressure, as compared to the high pressure case considered in the earlier study [5], the ion-neutral mean free path λ, due to resonant or near-resonant charge transfer, is approximately a constant. The ion mobility in this case can be found as [12]

$$\mu_+ = \frac{2e\lambda}{\pi M|\mathrm{u}|}, \tag{2.4}$$

where e and M are the ion charge and mass. By setting the ion flux (2.1) equal to $n\mathrm{u}$, we can find the ion drift velocity

$$|u| = \left(\frac{2e\lambda|\nabla\Phi|}{\pi M}\right)^{1/2}. \tag{2.5}$$

Following [9], we introduce nondimensional position and potential variables

$$\xi = \frac{x - l_-}{l_p - l_-}, \quad \eta = -\frac{\Phi}{T_e}. \tag{2.6}$$

The electropositive region extends from $x = l_-$, the edge of the electronegative region, to $x = l_p > l_-$, the plasma sheath edge. From equation (2.2) it follows that

$$\eta = -\ln\frac{n}{n_{e0}}. \tag{2.7}$$

Substituting (2.1), (2.2), (2.4) and (2.5) into (2.3) leads to the following differential equation for one dimensional rectangular coordinates:

$$\frac{d^2\eta}{d\xi^2} - 2\left(\frac{d\eta}{d\xi}\right)^2 = 2\beta\left(\frac{d\eta}{d\xi}\right)^{1/2}, \tag{2.8}$$

where

$$\beta = \left\{\frac{\pi(l_p - l_-)}{2\lambda}\right\}^{1/2} \frac{\nu_{iz}(l_p - l_-)}{u_{B0}} \tag{2.9}$$

and $u_{B0} = (eT_e/M)^{1/2}$ is the Bohm speed. With the substitution

$$\frac{d\eta}{d(\beta^{2/3}\xi)} = \chi, \tag{2.10}$$

(χ is a normalized electric field), (2.8) can be transformed to

$$\frac{d\chi}{2\chi^{1/2}(1+\chi^{3/2})} = d(\beta^{2/3}\xi). \tag{2.11}$$

A further integration yields

$$\frac{1}{6}\ln\frac{(\chi^{1/2}+1)^3}{\chi^{3/2}+1} + \frac{1}{\sqrt{3}}\arctan\frac{2\chi^{1/2}-1}{\sqrt{3}} = \beta^{2/3}\xi + C_1. \tag{2.12}$$

Combining (2.10) and (2.11) and integrating, we find

$$\frac{1}{3}\ln(1+\chi^{3/2}) = \eta + C_2. \tag{2.13}$$

Equations (2.12) and (2.13) provide a solution to (2.8) in a parametric form (χ serves as the parameter) with two constants of integration C_1 and C_2 to be determined from boundary conditions.

When considering the boundary conditions, it is convenient to have an expression for χ in terms of the ion drift velocity u. Using the normalizations (2.6) and substituting χ from (2.10) into (2.5), we obtain

$$\chi = \beta^{-2/3}\left\{\frac{\pi(l_p - l_-)}{2\lambda}\right\}w^2,$$

where $w = u(x)/u_{B0}$ is the normalized flow velocity. Substituting β from (2.9) into the preceding expression gives

$$\chi = a^{-2/3}w^2, \tag{2.14}$$

where

$$a = 2\nu_{iz}\lambda/\pi u_{B0}. \tag{2.15}$$

At the plasma sheath edge, the ions reach the Bohm speed, and their concentration is n_s. Using this boundary condition in (2.13) with χ obtained from (2.14) at $w = 1$ and η given by (2.7) determines

$$C_2 = \frac{1}{3}\ln(1 + a^{-1}) + \ln\frac{n_s}{n_{e0}}.$$

Substituting C_2 into (2.13) and using (2.7) and (2.14) we have

$$\frac{n_s}{n(x)} = \left\{\frac{a + w(x)^3}{a+1}\right\}^{1/3}, \tag{2.16}$$

which can be used to find the ratio of the density to the density at the sheath edge in terms of the ratio of the ion drift velocity to the Bohm speed. In particular, for an electropositive region with an entering velocity u_{in} and a density n_{e0} at $x = \ell_-$, the ratio of n_s/n_{e0} is then

$$\frac{n_s}{n_{e0}} = \left\{\frac{a + w_0^3}{a+1}\right\}^{1/3} \tag{2.17}$$

where $w_0 = u_{in}/u_{B0}$. If u_{in} and the electron temperature T_e, and therefore ν_{iz} and u_{B0}, are known, then (2.17) gives n_s/n_{e0}.

At the edge of the electronegative region, the ions enter the electropositive region with the velocity u_{in}. With χ obtained from (2.14) at $w = w_0$, we find from (2.12) that

$$C_1 = \frac{1}{6}\ln\frac{\{a^{1/3} + w_0\}^3}{a + w_0^3} + \frac{1}{\sqrt{3}}\arctan\frac{2w_0 - a^{1/3}}{\sqrt{3}a^{1/3}}.$$

Substituting C_1 into (2.12) yields

$$\frac{1}{6}\ln\frac{\{a^{1/3} + w\}^3}{a + w^3} + \frac{1}{\sqrt{3}}\arctan\frac{2w - a^{1/3}}{\sqrt{3}a^{1/3}} - \frac{1}{6}\ln\frac{\{a^{1/3} + w_0\}^3}{a + w_0^3}$$

$$-\frac{1}{\sqrt{3}}\arctan\frac{2w_0 - a^{1/3}}{\sqrt{3}a^{1/3}} = \frac{\pi(l_p - l_-)}{2\lambda}a^{2/3}\xi, \tag{2.18}$$

which implicitly gives the ratio w of the ion velocity to the Bohm speed in terms of normalized position ξ. At the plasma sheath edge, $x = l_p$, $w = 1$ and $\xi = 1$, and equation (2.18)

yields the important relation

$$\frac{1}{6}\ln\frac{\{a^{1/3}+1\}^3}{a+1}+\frac{1}{\sqrt{3}}\arctan\frac{2-a^{1/3}}{\sqrt{3}a^{1/3}}-\frac{1}{6}\ln\frac{\{a^{1/3}+w_0\}^3}{a+w_0^3}$$

$$-\frac{1}{\sqrt{3}}\arctan\frac{2w_0-a^{1/3}}{\sqrt{3}a^{1/3}}=\frac{\pi(l_p-l_-)}{2\lambda}a^{2/3} \tag{2.19}$$

which can be solved simultaneously with global particle balance equations in the bulk of a discharge for T_e, u_{in}, and l_-, as described in the following section.

III. Three Species Electronegative Core

In this model [5], we consider a subset of charged particle species in a parallel plane geometry, and determine the spatially varying profiles of the species. As in electropositive plasmas, for each charged species we write a flux equation

$$\Gamma_i = -D_i\nabla n_i \pm n_i\mu_i E_i, \tag{3.1}$$

where $D_i = eT_i/m_i\nu_i$, $\mu_i = |q_i|/m_i\nu_i$, with ν_i the total momentum transfer collision frequency, T_i is the species temperature in volts, and the $\pm$ corresponds to positive and negative carriers, respectively. In equilibrium the sum of the currents must balance,

$$\sum_{i=1}^{N} q_i\Gamma_i = 0. \tag{3.2}$$

Assuming that both the negative ions and the electrons are in Boltzmann equilibrium, then

$$\frac{\nabla n_-}{n_-} = \gamma\frac{\nabla n_e}{n_e}, \tag{3.3}$$

where $\gamma = T_e/T_i$ (T_i is the common temperature of both ionic species). We assume $\gamma \gg 1$. Using charge neutrality and the Einstein relations,

$$\frac{D_-}{D_+} = \frac{\mu_-}{\mu_+} \quad , \quad \frac{D_e}{D_+} = \gamma\frac{\mu_e}{\mu_+}, \tag{3.4}$$

together with (3.1)–(3.3), we obtain an ambipolar diffusion coefficient for the positive ions [13]

$$D_{a+} = D_+ \frac{(1+\gamma+2\gamma\alpha)\left(1+\alpha\frac{\mu_-}{\mu_e}\right)}{(1+\gamma\alpha)\left(1+\frac{\mu_+}{\mu_e}(1+\alpha)+\frac{\mu_-}{\mu_e}\right)}, \tag{3.5}$$

where $\alpha = n_-/n_e$. Since μ_-/μ_e, $\mu_+/\mu_e \ll 1$, for all reasonable cases the second parentheses in both the numerator and denominator are approximately equal to one, yielding the simpler form

$$D_{a+} \approx D_+ \frac{1+\gamma+2\gamma\alpha}{1+\gamma\alpha}. \tag{3.6}$$

The structure of D_{a+} is easily seen from (3.6). For $\alpha \gg 1$, γ cancels such that $D_{a+} \approx 2D_+$. When α decreases below 1, but $\gamma\alpha \gg 1$, $D_{a+} \approx D_+/\alpha$ such that D_{a+} increases inversely with decreasing α. For $\gamma\alpha < 1$, $D_{a+} \approx \gamma D_+$, which is the usual ambipolar diffusion without negative ions. For plasmas in which $\alpha \gg 1$ at the plasma center, the entire transition region takes place over a small range of $1/\gamma < \alpha < 1$, such that the simpler value of $D_{a+} = 2D_+$ holds over most of the plasma. The thinness of the transition region allows us to separate the plasma into an electronegative core and an electropositive edge.

Consider now the positive ion diffusion equation, keeping only the dominant reaction rate constants. In plane-parallel geometry, we have

$$-\frac{d}{dx}\left(D_{a+}(\alpha)\frac{dn_+}{dx}\right) = K_{iz}n_0 n_e - K_{rec}n_+ n_-, \tag{3.7}$$

where n_0 is the neutral gas density, and K_{iz} and K_{rec} are the ionization and recombination reaction rate constants. We can eliminate n_e and n_- using the Boltzmann relation relating electron and ion densities $(n_e/n_{e0}) = (n_-/n_{-0})^{1/\gamma}$ and the "plasma approximation" of charge neutrality $n_+ = n_- + n_e$, to obtain

$$n_+ = n_- + n_{e0}\left(\frac{n_-}{n_{-0}}\right)^{1/\gamma}. \tag{3.8}$$

Substituting (3.8) into (3.7), we obtain the ion diffusion equation in terms of α, alone,

$$-\frac{d}{dx}\left[D_{a+}(\alpha)\frac{d}{dx}\left((\alpha+1)\left(\frac{\alpha}{\alpha_0}\right)^{\frac{1}{\gamma-1}}\right)\right] = K_{iz}n_0\left(\frac{\alpha}{\alpha_0}\right)^{\frac{1}{\gamma-1}} - K_{rec}n_{e0}\alpha\left((\alpha+1)\left(\frac{\alpha}{\alpha_0}\right)^{\frac{2}{\gamma-1}}\right) \tag{3.9}$$

where $D_{a+}(\alpha)$ is given by (3.6). Equation (3.9) is a function of three parameters: $\alpha_0 = n_{-0}/n_{e0}$, n_{e0}, and T_e. Because $\gamma \gg 1$ we see from (3.8) that $n_e \simeq n_{e0}$ in the electronegative core and that we can generally take $(\alpha/\alpha_0)^{\frac{1}{\gamma-1}} = 1$ in (3.9).

At lower pressures, for which the mobility is not constant in the electropositive portion of the discharge, as treated in Section II, the diffusion equation (3.9) does not describe this portion of the discharge. To make the problem tractable, we break up the discharge into a core electronegative region and an edge electropositive region. The transition takes place (nominally) at a position $x = \ell_-$ where $\alpha\gamma \sim 1$, which for most approximations can be taken to be equivalent to $\alpha = 0$. With this value ℓ_- we can write the conservation equation for positive ions in the electronegative core as:

$$\Gamma_+(\ell_-) = \int_0^{\ell_-} K_{iz}n_0n_e dx - \int_0^{\ell_-} K_{rec}n_+n_- dx. \tag{3.10}$$

The negative ion particle balance within the entire discharge is

$$\int_0^{\ell_p} K_{att}n_0n_e dx - \int_0^{\ell_-} K_{rec}n_+n_- dx = 0, \tag{3.11}$$

where K_{att} is the attachment reaction rate constant. The reaction rate constants are in general functions of the electron temperature T_e. The ion flux on the left hand side of (3.10) can be written as

$$\Gamma_+ = n_+u_+, \tag{3.12}$$

where u_+ is the local ion velocity, which is subject to the condition [14, 15]

$$u_+(x) \leq u_B(\alpha) \equiv \left[\frac{eT_i}{M_+}\frac{(\alpha+1)}{(\alpha+1/\gamma)}\right]^{1/2}, \tag{3.13}$$

i.e. that the local ion velocity u_+ is less than the local sound velocity u_B in an electronegative plasma. If the equality is reached, sufficient electric field builds up to decrease the negative ion density to a small value such that the sound velocity is not exceeded. For α large, ℓ_- occurs at the plasma edge such that $\ell_- = \ell_p$.

Assuming n_0 and n_{e0} are known, and that the density in the electropositive region at the border between the two regions is $n_+ \simeq n_{e0}$ ($\alpha \simeq 0$), then (3.10), (3.11) and (2.19) can be solved simultaneously with the diffusion equation (3.9), using the equality in (3.13) if it applies, to obtain the three unknown constants, α_0, T_e, and ℓ_-. The power absorbed by the electrons is then obtained from

$$P_{abs} = 2\mathcal{E}_c \int_0^{\ell_p} K_{iz} n_0 n_e dx + 2\mathcal{E}_w n_+(\ell_p) u_B. \tag{3.14}$$

where $\mathcal{E}_c$ is the collisional energy lost per electron-positive ion pair created, a known function of T_e, and $\mathcal{E}_w$ is the kinetic energy lost per electron-ion pair lost to the wall. If the electron power is given, (3.14) becomes an additional equation to be solved simultaneously for the additional constant n_{e0}.

Although we have derived a set of equations that are considerably simplified from the coupled three-species equations, they involve a nonlinear differential equation (3.9) in the electronegative core coupled to a set of equations involving both transcendental functions and integrals. In the next section we describe some approximations that reduce the equations to a simpler set which, in some instances, may be solved analytically by iterating on weakly varying parameters.

IV. Approximate Solutions

We found in [5], that the negative ion profile in an electronegative region could be reasonably approximated by a parabola, provided α_0 was neither too large or too small, as described below. Since the conservation laws are expressed as integrals over the profiles,

the macroscopic plasma parameters are relatively insensitive to exact shape of the profile. Provided $\alpha_0 \gg 1$, only a narrow region at the edge of the electronegative plasma has a diffusion coefficient that is varying. Since we match the flux $\Gamma_+ = -D_{a+}dn_+/dx$ leaving the electronegative plasma, to that entering the electropositive plasma, we can see from (3.10) that this depends only on integrals over the entire electronegative region, rather than the rapidly varying $D_{a+}(\alpha)$ and dn_+/dx, separately. This allows us to match the electronegative solution to the electropositive solution with discontinuities in D_{a+} and dn_+/dx.

A. *Parabolic Models without Ion Sound Limitation*

Consider, as in previous work [5], that an electronegative core region of the discharge exists in which α is sufficiently large that $D_{a+} \approx \bar{D}_{a+}$, a constant, that $n_e \approx n_{e0}$, a constant, and that the effect of positive-negative ion recombination can be neglected in determining the spatial distribution. The diffusion equation (3.9) then takes the simple form

$$-\bar{D}_{a+}\frac{d^2\alpha}{dx^2} = K_{iz}n_0.$$

In this approximation $n_+(x)$ has a simple parabolic solution of the form

$$\frac{n_+}{n_{e0}} = \frac{n_-}{n_{e0}} + 1 = \alpha_0\left(1 - \frac{x^2}{\ell^2}\right) + 1, \tag{4.1}$$

where ℓ is the scale length of the parabola. We assume that $\ell_- = \ell$ since there is no ion sound limitation. The diffusion coefficient $\bar{D}_{a+}$ is obtained by averaging α in (3.6) over a parabola

$$\bar{D}_{a+} = D_+\frac{1+\gamma+2\gamma\bar{\alpha}}{1+\gamma\bar{\alpha}} \tag{4.2}$$

where in rectangular coordinates $\bar{\alpha} = \frac{2}{3}\alpha_0$.

Substituting (4.1) and (4.2) in (3.10) and (3.11) and integrating, we obtain, respectively,

$$K_{iz}n_0\ell = K_{rec}n_{e0}\left(\frac{8}{15}\alpha_0^2 + \frac{2}{3}\alpha_0\right)\ell + \frac{2\bar{D}_{a+}\alpha_0}{\ell}, \tag{4.3}$$

$$K_{att}n_0\ell_p = K_{rec}n_{e0}\left(\frac{8}{15}\alpha_0^2 + \frac{2}{3}\alpha_0\right)\ell, \tag{4.4}$$

where in (4.3) the integration is only over the strongly electronegative plasma, and in (4.4) we approximate $n_e \approx n_{e0}$ everywhere as discussed in the introduction (see also numerical comparisons, which show that the profiles from Sec. II are relatively flat, such that results obtained from integrals over those profiles are not greatly different from the results obtained by integrals over a constant profile). At $x = \ell$ this electronegative solution is matched to an electropositive edge solution. The electropositive solution could be a sinusoidal profile, at higher pressures, the more nearly constant profile, obtained in Section II, at lower pressures, or a profile intermediate between the two. In previous work [5] a parabolic profile was assumed in the electropositive region also, and the fluxes matched at the interface between the regions, to solve for the ratio ℓ/ℓ_p. The analysis is simplified by assuming that n_{e0} is known. The absorbed electron power P_{abs} is then obtained *a posteriori* from (3.14). If P_{abs} is specified rather than n_{e0}, then n_{e0} can be obtained iteratively, as is done for T_e, as described below. Assuming n_{e0} is known, we then solve (4.3), (4.4), and (2.19) simultaneously for T_e, α_0, and ℓ, where in (2.19) $u_{in} = 2\bar{D}_{a+}\alpha_0/\ell$.

We can further approximate the equations to obtain a set that may be iteratively solved analytically. First we note that (4.4) can be solved for α_0, assuming that ℓ/ℓ_p is known, to obtain

$$\alpha_0 = -\frac{5}{8} + \sqrt{\left(\frac{5}{8}\right)^2 + \frac{15}{8}\frac{K_{att}}{K_{rec}}\frac{n_0}{n_{e0}}\frac{\ell_p}{\ell}}. \tag{4.5a}$$

For large α_0 this reduces to

$$\alpha_0 \approx \left(\frac{15}{8}\frac{K_{att}}{K_{rec}}\frac{n_0}{n_{e0}}\frac{\ell_p}{\ell}\right)^{1/2}. \tag{4.5b}$$

Since ℓ/ℓ_p is near unity for large α_0, the weak dependence on ℓ_p/ℓ is not significant; once a complete solution is found, the value of α_0 can be improved by iteration. Equation (4.5b) exhibits the important scaling $\alpha_0 \propto (n_0/n_{e0})^{1/2}$. Making the assumption that the density

in the electropositive solution is relatively constant, except very near the sheath, such that n_e can be set equal to n_{e0} in the ion flux balance equation, the positive ion particle balance in the electropositive region is

$$\frac{2\bar{D}_{a+}\alpha_0}{\ell} + K_{iz}n_0(\ell_p - \ell) = h_\ell u_{B0}, \tag{4.6}$$

where $u_{B0} = (eT_e/M)^{1/2}$, and where $h_\ell \equiv n_s/n_{e0}$ can be obtained from (2.17). As in previous work [5], the temperature sensitive term K_{iz} can be eliminated by substituting K_{iz} from (4.3) into (4.6) to obtain

$$2\bar{D}_{a+}\alpha_0\frac{\ell_p}{\ell^2} + K_{rec}n_{e0}\left(\frac{8}{15}\alpha_0^2 + \frac{2}{3}\alpha_0\right)(\ell_p - \ell) = h_\ell u_{B0}. \tag{4.7}$$

We note that $\bar{D}_{a+}$, K_{rec}, and u_{B0} and h_ℓ are only weakly dependent on T_e, such that the temperature evaluation can be essentially decoupled from the evaluation of α_0 and ℓ. In this approximation, with an assumed T_e, (4.5) and (4.7) can be solved for α_0 and ℓ, with h_ℓ given in some approximation from (2.17). For example, solving explicitly for ℓ/ℓ_p in terms of α, from (4.7), and using (4.4) to simplify, we have

$$\frac{\ell}{\ell_p} = \frac{K_{att}n_0 + \sqrt{(K_{att}n_0)^2 + \dfrac{8\bar{D}_{a+}\alpha_0}{\ell_p^2}\left(\dfrac{h_\ell u_{B0}}{\ell_p} + K_{att}n_0\right)}}{2\left(\dfrac{h_\ell u_{B0}}{\ell_p} + K_{att}n_0\right)}. \tag{4.8}$$

which is valid provided that $\ell/\ell_p < 1$ and that the ion drift velocity is less than the ion sound velocity. A simple hand calculation then allows an iterative solution using (4.5) and (4.8). We also note the important limiting cases: (1) if the recombination flux is much less than the diffusion flux, i.e. $K_{att}n_0 \ll h_\ell u_{B0}/\ell_p$ then

$$\frac{\ell}{\ell_p} \simeq \frac{(2\bar{D}_{a+}\alpha_0/\ell_p)^{1/2}}{(h_\ell u_{B0})^{1/2}}$$

or, substituting ℓ for ℓ_p on the right hand side,

$$\frac{\ell}{\ell_p} \simeq \frac{(2\bar{D}_{a+}\alpha_0/\ell)}{(h_\ell u_B)}. \tag{4.9}$$

We see that ℓ/ℓ_p is linearly related to the ratio of the ion diffusion out of the electronegative region to the total ion diffusion. (2) In the opposite limit of $K_{att}n_0 \gg h_\ell u_{B0}/\ell_p$, $\ell/\ell_p \simeq 1$. To solve for the temperature by iteration, we add (4.3) and (4.6), and substituting from (4.4), as previously, we obtain

$$K_{iz}n_0\ell_p - K_{att}n_0\ell_p = h_\ell u_{B0} \tag{4.10}$$

which can be solved explicitly for K_{iz}, if K_{att}, h_ℓ and u_{B0} are known. Since these are weak functions of T_e, while K_{iz} is a strong function of T_e the procedure updates T_e.

B. *Parabolic Model with an Ion Sound Limitation*

Depending on plasma parameters, it is possible to reach the local ion sound velocity in the electronegative region. In this case, if we use the parabolic approximation for negative ions the electronegative region terminates abruptly at a position $\ell_- < \ell$. It is shown in [10] that an internal nonneutral transition region forms. The transition from an electronegative core to an electropositive edge region takes place over a few electron Debye lengths, which is the basis for our assumption of an abrupt transition. The positive ion flux is continuous, but the positive and negative ion densities and the positive ion velocity change abruptly. The electric fields that build up inside this nonneutral region are small. They are sufficient to confine the negative ions, but not the electrons. Hence the electron density changes only slowly within this region. The particle balance equation for positive ions is then

$$\begin{aligned} K_{iz}n_0n_{e0}\ell_- =& K_{rec}n_{e0}^2\left\{\alpha_0^2\ell_-\left(1-\frac{2}{3}\frac{\ell_-^2}{\ell^2}+\frac{1}{5}\frac{\ell_-^4}{\ell^4}\right)+\alpha_0\ell_-\left(1-\frac{1}{3}\frac{\ell_-^2}{\ell^2}\right)\right\} \\ &+ n_{e0}\left[\alpha_0\left(1-\frac{\ell_-^2}{\ell^2}\right)+1\right]u_B \end{aligned} \tag{4.11}$$

where $u_B(\alpha_-)$ is given by (3.13), with

$$\alpha_- = \alpha_0(1 - \ell_-^2/\ell^2). \tag{4.12}$$

The negative ion particle balance is

$$K_{att} n_0 n_{e0} \ell_p = K_{rec} n_{e0}^2 \left\{ \quad \cdot \quad \right\}, \tag{4.13}$$

with the $\{ \cdot \}$ repeated from (4.11). We note that the last term in (4.11) is $n_{e0} u_{in}$, defined in (2.19) as $w_0 = u_{in}/u_{B0}$. Therefore (2.19) must be solved simultaneously with (4.11)–(4.13) and (3.13) to determine α_0, α_-, ℓ_-, ℓ, and T_e.

As described in Sec. IV-A, the equations for the electronegative region can be connected to the approximate electropositive equations. Equation (4.6) becomes

$$\frac{2\bar{D}_{a+}\alpha_0 n_{e0}}{\ell^2}\ell_- + K_{iz} n_0 n_{e0}(\ell_p - \ell_-) = n_{e0} h_\ell u_{B0} \tag{4.14}$$

with h_ℓ given by (2.17). As previously, the temperature sensitive rate constant K_{iz} can be eliminated from (4.14) using (4.11) to obtain

$$\frac{2\bar{D}_{a+}\alpha_0 n_{e0}}{\ell^2}\ell_- + K_{rec} n_{e0}^2 \left\{ \quad \cdot \quad \right\} \left(\frac{\ell_p}{\ell_-} - 1 \right) +$$

$$n_{e0} \left[\alpha_0 \left(1 - \frac{\ell_-}{\ell^2} \right) + 1 \right] u_{B0} \left(\frac{\ell_p}{\ell_-} - 1 \right) = n_{e0} h_\ell u_{B0}. \tag{4.15}$$

Using the negative ion particle balance (4.13), (4.15) can be more simply written as

$$\frac{2\bar{D}_{a+}\alpha_0 n_{e0}\ell_p}{\ell^2} + K_{att} n_0 n_{e0} \ell_p \left(\frac{\ell_p}{\ell_-} - 1 \right) = h_\ell n_{e0} u_{B0} \tag{4.16}$$

The additional equation that is required to solve for the new variable ℓ_- is the condition at which local sound speed is attained within the electronegative region. From the flux condition this occurs when

$$\frac{2\bar{D}_{a+}\alpha_0 n_{e0}\ell_-}{\ell^2} = \left[\alpha_0 \left(1 - \frac{\ell_-^2}{\ell^2} \right) + 1 \right] n_{e0} u_B(\alpha) \tag{4.17}$$

The left hand side is the flux, which depends only weakly on the local $\alpha(\ell_-)$ while the terms on the right hand side depend strongly on $\alpha(\ell_-)$. Equations (4.13), (4.14), (4.16), and (4.17) are solved simultaneously for α_0, ℓ, ℓ_-, and T_e with n_0 and n_{e0} as parameters. Alternatively T_e is assumed, then (4.13), (4.16), and (4.17) are solved for α_0, ℓ, and ℓ_p, and T_e is then obtained from (4.14) with the solution improved by iteration. We note that in (4.14) and (4.16), $u_{B0} = (eT_e/M)^{1/2}$, the usual Bohm velocity when $\alpha = 0$. As α_0 increases, there is a transition to a single region electronegative plasma when $\ell_- = \ell_p$. In this case (4.11) and (4.13) still hold with ℓ_p replacing ℓ_-. The third equation to complete the set is flux balance at the sheath edge, which is given by (4.17) with ℓ_p replacing ℓ_-. This high α_0 case is treated in a separate paper dealing with another set of issues, so we do not consider it further here.

Returning to examination of condition (4.17) more closely, we set $2\bar{D}_{a+} = 4D_+$, for simplicity and approximating u_B by

$$u_B = v_{Ti}\left(\frac{1+\alpha}{\alpha}\right)^{1/2}, \tag{4.18}$$

then (4.17) yields a cubic equation for ℓ_-^2/ℓ^2:

$$\left(\frac{4\lambda}{\ell}\right)^2 \alpha_0^3 \frac{\ell_-^2}{\ell^2}\left(1-\frac{\ell_-^2}{\ell^2}\right) = \left[1+\alpha_0\left(1-\frac{\ell_-^2}{\ell^2}\right)\right]^3, \tag{4.19}$$

where we have substituted $D_+ = v_{Ti}\lambda$. For small α_0 we find numerically that (4.19) has no real solutions, while for larger α_0 (4.19) has two positive real solutions, with the solution with the smaller value of ℓ_-/ℓ giving the transition between the electronegative and electropositive regions. If there are no solutions to (4.19), then we are back to the case treated in Sec. IV-A with $\ell_- = \ell$ (the scale length of the parabola is equal to the size of the electronegative region). In Fig. 2 we plot α_- vs α_0 with $g = (4\lambda/\ell)^2$ a parameter. We

see the basic structure of the solution as described above. For a given electronegativity α_0, we see that there is an ion sound limitation for λ/ℓ sufficiently large (low pressure).

If there is a solution to (4.19) we can drop the small terms linear in α_0 in (4.13) to obtain the approximate scaling of α_0:

$$\alpha_0 = \left(\frac{K_{att} n_0 \ell_p}{K_{rec} n_{e0} \ell_-}\right)^{1/2} \left(1 - \frac{2}{3}\frac{\ell_-^2}{\ell^2} + \frac{1}{5}\frac{\ell_-^4}{\ell^4}\right)^{-1/2} . \tag{4.20}$$

Since ℓ_-/ℓ changes slowly with parameters, we find that the scaling of α_0 in (4.20) is approximately the same as that in (4.5b), without the ion sound limitation. In fact, $\ell_-/\ell \simeq 1$ for most cases such that (4.5b) is recovered.

Although the ion sound limitation is a physical phenomenon, the detailed way in which it manifests itself within the discharge cannot be obtained within diffusion theory. We compare the results of the two parabolic approximations, with and without the ion sound limitation, in the numerical calculations of Sec. V. We see there that both approximations give similar values of α_0 and T_e.

V. Numerical Results

For our numerical examples we consider an oxygen feedstock gas. We use oxygen because the reaction rates are reasonably well known, and because PIC Monte-Carlo simulations have been done using these rates. However, because our theory has been developed for a three species plasma, (as has the comparison PIC codes) we do not consider dissociation of O_2 to O. This is reasonable for low electron density (low power) discharges that we consider in the examples, but limits the applicability of the model in real oxygen discharges. However, with other reaction rates, the model can be applied to other feedstock gases, such as chlorine, which do have large parameter ranges with three plasma species.

For our analysis we use the following, somewhat simplified, reaction rates, that have been constructed by integration of Maxwellian distributions over cross sections [16, 11]

$$K_{iz} = 2.13 \cdot 10^{-14} \exp(-14.5/T_e) \quad \mathrm{m}^3/\mathrm{s} \tag{5.1}$$

$$K_{att} = 7.89 \cdot 10^{-17} \exp(-3.07/T_e) \quad \mathrm{m}^3/\mathrm{s} \tag{5.2}$$

$$K_{rec} = 1.4 \cdot 10^{-13} \quad \mathrm{m}^3/\mathrm{sec} \tag{5.3}$$

$$\sigma_{mi} = 5 \cdot 10^{-19} \quad \mathrm{m}^2, \tag{5.4}$$

where K_{iz}, K_{att}, and K_{rec} are rate constants and σ_{mi} is the cross section for the reactions

$$O_2 + e \rightarrow O_2^+ + 2e, \quad \text{(ionization)} \tag{5.5}$$

$$O_2 + e \rightarrow O^- + O, \quad \text{(dissociative attachment)} \tag{5.6}$$

$$O_2^+ + O^- \rightarrow O_2 + O, \quad \text{(recombination)} \tag{5.7}$$

$$O_2^+ + O_2 \rightarrow O_2^+ + O_2, \quad \text{(scattering)} \tag{5.8a}$$

$$O_2^+ + O_2 \rightarrow O_2 + O_2^+, \quad \text{(charge exchange)} \tag{5.8b}$$

$$O^- + O_2 \rightarrow O^- + O_2. \quad \text{(scattering)} \tag{5.8c}$$

The latter three reactions with momentum transfer cross section σ_{mi} lead to effective diffusion coefficients for positive and negative ion species. The mean free path is then given as

$$\lambda = \frac{1}{n_0 \sigma_{mi}}. \tag{5.9}$$

The rate constant for charge transfer of O^- on O_2 is small because the threshold energy required for this process is ~ 1.0 eV, which is much higher than the thermal energy of the heavy particles; hence this process is unimportant. The simulations include many other reactions, e.g. vibrational excitations, which mainly go into the calculation of the energy loss per ionization, which we will take here as a known quantity.

We obtain plasma parameters for two values of the gas pressure $p = 50$ mTorr and $p = 10$ mTorr. The former corresponds to a transition region between a pressure sufficiently high that a constant mobility can be used in the electropositive edge region and the lower pressure regime considered in this paper. It was the principal example used in our previous study [5].

The latter pressure well satisfies the low pressure constant mean free path approximation in the electropositive edge, as assumed here. For later comparison with PIC simulations we use slightly different plasma half-widths at the two pressures $\ell_p = 1.25$ cm at $p = 50$ mTorr and $\ell_p = 1.8$ cm at $p = 10$ mTorr, both in the large aspect ratio parallel plane approximation. In all calculations we take n_{e0} as the input control variable.

In Fig. 3 with $p = 50$ mTorr and $n_{e0} = 2.6 \cdot 10^9$ cm^{-3}, we compare the profiles, using our complete model, Eqs. (2.19), (4.3), and (4.4) without the ion sound limitation, and Eqs. (2.19), (4.11), (4.13), and (4.17) with the ion sound limitation. As expected, we see the truncation of the electronegative region when the ion sound limitation is applied. However, the values of the parameters α_0 and T_e are quite similar in the two cases, as is the average electronegativity over the profiles, α_{ave}. In Fig. 4 the profiles in the two approximations are again compared at the lower pressure of $p = 10$ mTorr and at a higher density of $n_{e0} = 1.1 \cdot 10^{10}$ cm^{-3}, to significantly reduce the electronegativity. Again, the profiles are quite distinct, but the plasma parameters are similar. As described in Sec. IV, the profiles ignore the rapidly varying diffusion in the thin transition zones and ignore processes in the narrow nonneutral region, which, if included would keep both the density and slopes continuous. An integration of the diffusion equation (3.9), using a given value of T_e and α_0 shows this quite clearly in the case without the ion sound limitation, as shown in our previous work [5].

In Fig. 5 we compare the two approximations for varying n_{e0} at $p = 50$ mTorr. In Fig. 5a we plot α_0 vs n_{e0}; in Fig. 5b we plot T_e vs α_0, and in Fig. 5c we plot ℓ/ℓ_p (no sound speed limitation) and ℓ_-/ℓ_p (with a sound speed limitation) vs α_0. We can see the onset of the sound speed limitation with increasing α_0 (decreasing n_{e0}, at a given pressure, as expected from Fig. 2). Again, the average plasma parameters are little changed by the

inclusion of the ion sound speed limitation. In Fig. 6 we repeat the results of Fig. 5 for the lower pressure $p = 10$ mTorr, obtaining similar results. The ion sound limitation appears earlier, as can be shown by solving (4.19) for the critical case of a single solution (onset of ion sound limitation) as a function of the pressure, which in the limit of $4\lambda/\ell \ll 1$, is

$$\alpha_{0_{crit}} = \frac{3\sqrt{3}}{2}\frac{\ell}{4\lambda}. \tag{5.8}$$

In addition to the solution given above, we also have the more approximate solutions, which can be solved analytically by iteration. To see how close the approximate solutions based on (4.6) are to the more accurate solutions based on (2.19) given in Figs. 5 and 6, we compare the two solutions for ℓ/ℓ_p in Fig. 7 for the higher pressure case of $p = 50$ mTorr. For definiteness, we do this for the solutions without an ion sound limitation, using Eqs. (4.5a) and (4.8) together with (2.17) to solve iteratively for α_0 and ℓ with T_e given, and then using (4.10) to solve iteratively for T_e. The comparison with results repeated from Fig. 5 shows that the approximate equations give results reasonably close to those of the more complete equations.

Finally, in Fig. 8 we give results for the two PIC Monte-Carlo simulations. The details of the simulation are given in [11]. These simulations were also used in the comparison with the constant mobility model [5]. Comparing the results in Fig. 8a with the higher pressure case in Fig. 3 we see that the model gives a somewhat larger ℓ/ℓ_p and an α_0 larger by about a factor of two than the simulation. The larger ℓ/ℓ_p is due, in part, to the larger α_0. In our previous study [5], in which we also obtained a similarly larger value of α_0 in the modeling, we found that part of the discrepancy was due to a two temperature electron distribution in the PIC simulation. Introduction of a two temperature electron distribution into the model (which is rather straightforward to do), significantly reduced α_0, such that the ratio between the two values of α_0 was approximately 1.5. We discuss the discrepancies, further,

in Section VI. In Fig. 8a we also compare the PIC simulation profile to the profile (dashed curve) obtained by integration of (3.9) with the same α_0. There is some indication of the ion sound limitation, but it is mixed with the opposite effect of the changing $D_{a+}(\alpha)$ at the edge of the electronegative region. In Fig. 8b the profiles obtained from the simulation at the lower pressure $p = 10$ mTorr, higher electron density $n_{e0} = 1.1 \cdot 10^{10}$ cm^{-3} case correspond to the model results in Fig. 4. In Fig. 8b we again compare the simulation to the integration of (3.9) with the same α_0 (dashed curve). Comparing the profiles to the profiles in Fig. 4, obtained from the models, we see the same qualitative features as found for the higher pressure lower density case. The model α_0 is too large by about a factor of two, and there is some hint of the ion sound limitation in the simulation. The value of ℓ_-/ℓ_p in the simulation lies between the two model approximations. However, the region of the electronegative core where $\alpha \lesssim 1$ is a much larger fraction of the core, making the approximations more difficult to interpret.

VI. Conclusion and Discussion

We have developed the macroscopic equations that are required for determining the equilibrium of an electronegative plasma, based on the Thompson [13] form of the electronegative ambipolar diffusion coefficient which assumes that the negative ions are in Boltzmann equilibrium with the fields. The model separates the plasma into an electronegative core and an electropositive edge. The electropositive edge is treated by generalizing a constant mean-free-path model to include the flux from the core. The model results in an electron density in the core that is essentially clamped to a constant value. For this situation, provided the recombination flux does not dominate the wall flux, a parabolic approximation to the density profile can be made, leading to a simplified set of equations that can be treated fully analytically.

Over a range of parameters, the flux in the electronegative region is below the modified Bohm flux ($\Gamma_+ < nu_B$), allowing the matching of the electronegative plasma to the electropositive edge plasma at $\alpha = 0$. For other parameters $\Gamma_+ = nu_B$ within the electronegative region, resulting in an ion sound limitation to the flow. In this case the matching conditions are more complicated but can still be approximated with parabolic solutions. The results of the matching both including and ignoring the ion sound limitation are compared, giving similar macroscopic values of α_0 and T_e. The values of α_0, T_e, and ℓ_-/ℓ_p are obtained at two pressures, and for a wide range of electron densities for the two approximations.

The profiles obtained for the two model approximations were compared to PIC Monte-Carlo simulations, giving reasonable agreement but with values of α_0 which were a factor of two larger in the models. One reason for the discrepancy between the simulation and the theory is the tendency for low pressure capacitively coupled r.f. discharges, as used in the PIC simulation, to develop non-Maxwellian temperature distributions. In particular, efficient sheath heating tends to develop higher temperature tails to the distribution which effectively control the ionization rate. These distributions have been observed experimentally, and in both electropositive and electronegative plasma simulations [17, 11]. In our previous studies [5] we showed that about half of the discrepancy in α_0 could be accounted for by including a two-temperature distribution in the model. The remaining discrepancy could be accounted for by the manner in which the reaction rate coefficients are employed in the Monte-Carlo calculation. In this sense our analytic results are also a test of the simulation, and a resolution requires that both be tested against experiments.

For a fully self-consistent analytic model, a method for calculating the non-Maxwellian electron temperature will need to be devised. This is equally true for electropositive and

electronegative plasmas. In other types of discharges in which ohmic heating is the dominant heating mechanism, a single temperature Maxwellian may be a good approximation to the electron energy distribution function. In these situations, the analytic model developed here should describe the plasma equilibrium more adequately. Of course the ultimate tests of both analytic models and simulations are comparisons with experiments; we plan to make such comparisons in future work.

Acknowledgment

The authors wish to acknowledge the support of Department of Energy Grant DE-FG03-87ER13727, National Science Foundation Grant ECS-921750, Lawrence Livermore National Laboratory Grant PPRI-LLNL CP 94-06/B283626, and a gift from the Lam Research Corporation.

References

1. Edgley P D and Von Engel A 1980 *Proc. Roy. Soc.*, **A370**, 375 (London)
2. Ferreira C M, Gousset G and Touzeau M 1988 *J. Phys. D: Appl. Phys.*, **21**, 1403
3. Haas F A, Lea L M and Holmes A J T 1991 *J. Phys. D: Appl. Phys.*, **24**, 1541
4. Tsendin L D 1989 *Sov. Phys. Tech. Phys.*, **34**, 11
5. Lichtenberg A J, Vahedi V, Lieberman M A and Rognlien T 1994 *J. App. Phys.*, **75**, 2339
6. Ferreira C M and Gousset G 1991 *J. Phys. D: Appl. Phys.*, **24**, 775
7. Feaktistov V A, Lopnev D L, Klopovsky K S, Popov A M, Popovicheva O B, Rakhimov A T, and Rakhimova T V 1993 *J. Nucl. Materials*, **200**, 309
8. Lee C, Graves D B, Lieberman M A and Hess D W 1994 *J. Electrochemical Soc.*, **141**, 6; Lee C and Lieberman M A 1995 *J. Vac. Sci. and Tech.*, **A13**, 368
9. Godyak V A 1986 *Soviet Radio Frequency Discharge Research*, Delphic Associates,

Falls Church, VA

10. Kouznetsov I, Lichtenberg A J and Lieberman M A 1995 "Internal Sheaths in Low Pressure Electronegative Discharges," to be submitted to *IEEE Trans. on Plasma Science*
11. Vahedi V 1993 "Modeling and Simulation of R.F. Discharges Used for Plasma Processing," Ph.D Dissertation, University of California, Berkeley; Vahedi V, DiPeso G, Birdsall C K, Lieberman M A and Rognlien T D 1993 *Plasma Sources Science and Technology*, **2**, 261 and **2**, 273
12. Smirnov B M 1981 *Physics of Weakly Ionized Gases*, Mir, Moscow
13. Thompson J B 1959 Research Notes, *Proc. Royal Soc.*, **73**, 818; Rogoff G L 1985 *J. Phys. D: Appl. Phys.*, **18**, 1533
14. Braithwaite N St J and Allen J E 1988 *J. Phys. D: Appl. Phys.*, **21**, 1733
15. Boyd R L F and Thompson J B 1959 *Proc. Royal Soc.*, **A252**, 102; Rieman K-U 1991 *J. Phys. D: Appl. Phys.*, **24**, 493; Boswell R W, Lichtenberg A J and Vender D 1992 *IEEE Trans. on Plasma Sci.*, **20**, 62
16. e.g. see Mason E A and McDaniel E W 1988 *Transport Properties of Ions in Gases*, John Wiley; Phelps A V 1985 JILA Information Center Report 28, University of Colorado, Boulder
17. Wood B 1991 "Sheath Heating in Low Pressure Capacitive R.F. Discharges," Thesis, University of California, Berkeley

Figure Captions

Figure 1. Sketches of the two region plasma having an electronegative core and an electropositive edge: (a) without an ion sound speed limitation, (b) with an ion sound speed limitation on the velocity of the ions.

Figure 2. Values of α_- vs α_0 with $(4\lambda/\ell)^2$ as a parameter, which satisfy (4.19) for $u_+ = u_B$.

Figure 3. Density profiles from the complete model of an oxygen discharge with three species, for $\ell_p = 1.25$ cm, $p = 50$ mTorr, and $n_{e0} = 2.6 \cdot 10^9$ cm^{-3} (a) without and (b) with an ion sound speed limitation.

Figure 4. The same as Fig. 3 with $\ell_p = 1.8$ cm, $p = 10$ mTorr, and $n_{e0} = 1.1 \cdot 10^{10}$ cm^{-3}.

Figure 5. Plasma parameters variation with control parameter n_{e0} (explicitly or implicitly) for $\ell_p = 1.25$ cm and $p = 50$ mTorr. Results are given without ion sound speed limitation (solid line) and with limitation (dashed lines) for (a) α_0 vs n_{e0}; (b) T_e vs α_0; and (c) ℓ/ℓ_p vs α_0.

Figure 6. The same as Fig. 5 with $\ell_p = 1.8$ cm and $p = 10$ mTorr.

Figure 7. Comparison of results from complete model using (2.19) to describe the electropositive edge region, with the approximate solution assuming that $n_e = n_i = n_{e0}$ in the electropositive edge except at the transition with the sheath where $n_e = n_i = n_s$.

Figure 8. PIC simulations of profiles (solid lines) for (a) $\ell_p = 1.25$ cm, $p = 50$ mTorr, $n_{e0} = 2.6 \cdot 10^9$ cm^{-3}; and (b) $\ell_p = 1.8$ cm, $p = 10$ mTorr, $n_{e0} = 1.1 \cdot 10^{10}$ cm^{-3}. The dashed curves are integrations of (3.9) using the values of α_0 and T_e obtained from the simulations.

Fig. 1a

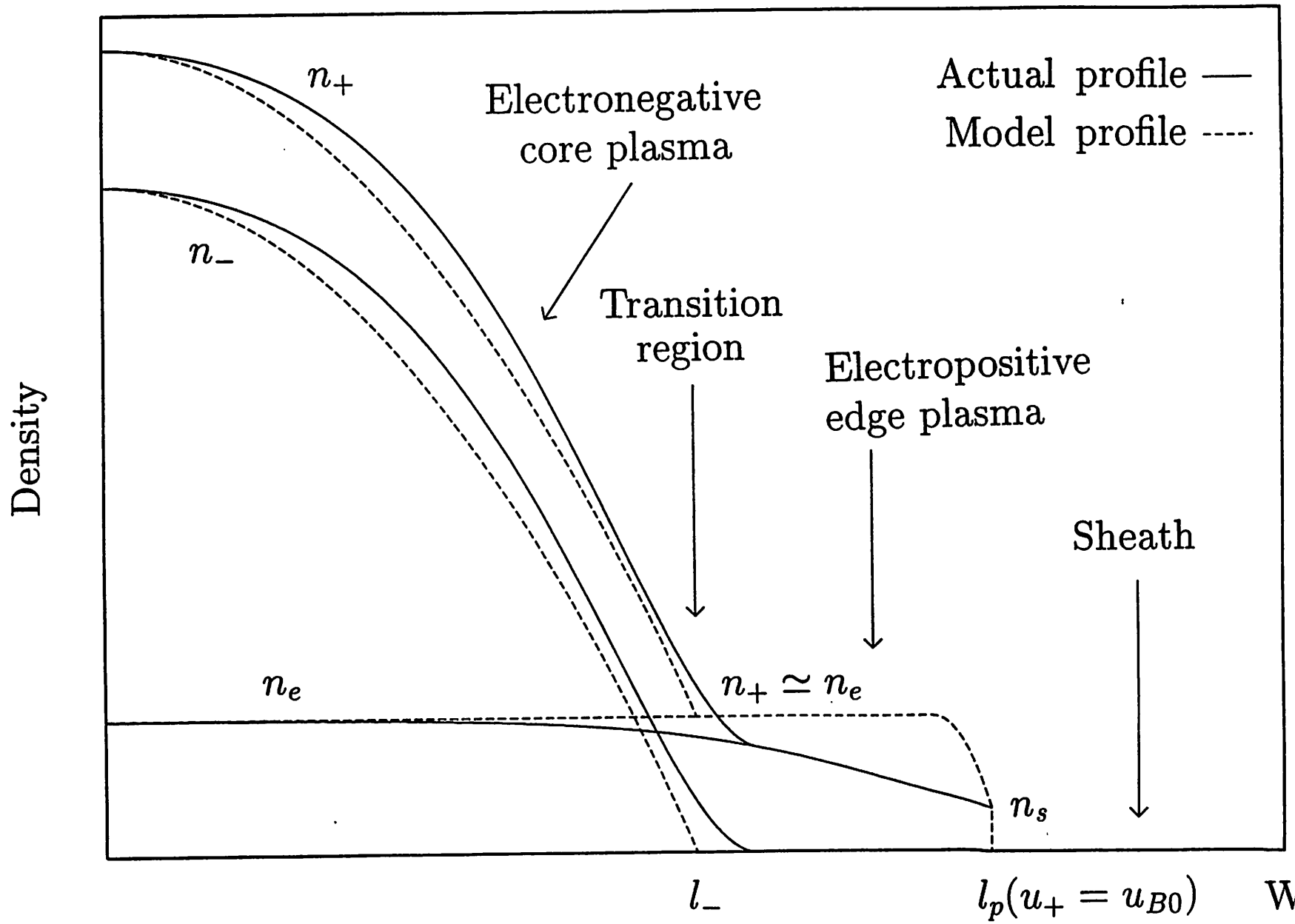
Actual profile —
Model profile -----
n_+
Electronegative
core plasma
n_-
Transition
region
Electropositive
edge plasma
Sheath
Density
n_e
$n_+ \simeq n_e$
n_s
l_-
$l_p(u_+ = u_{B0})$
Wall

Fig. 1b

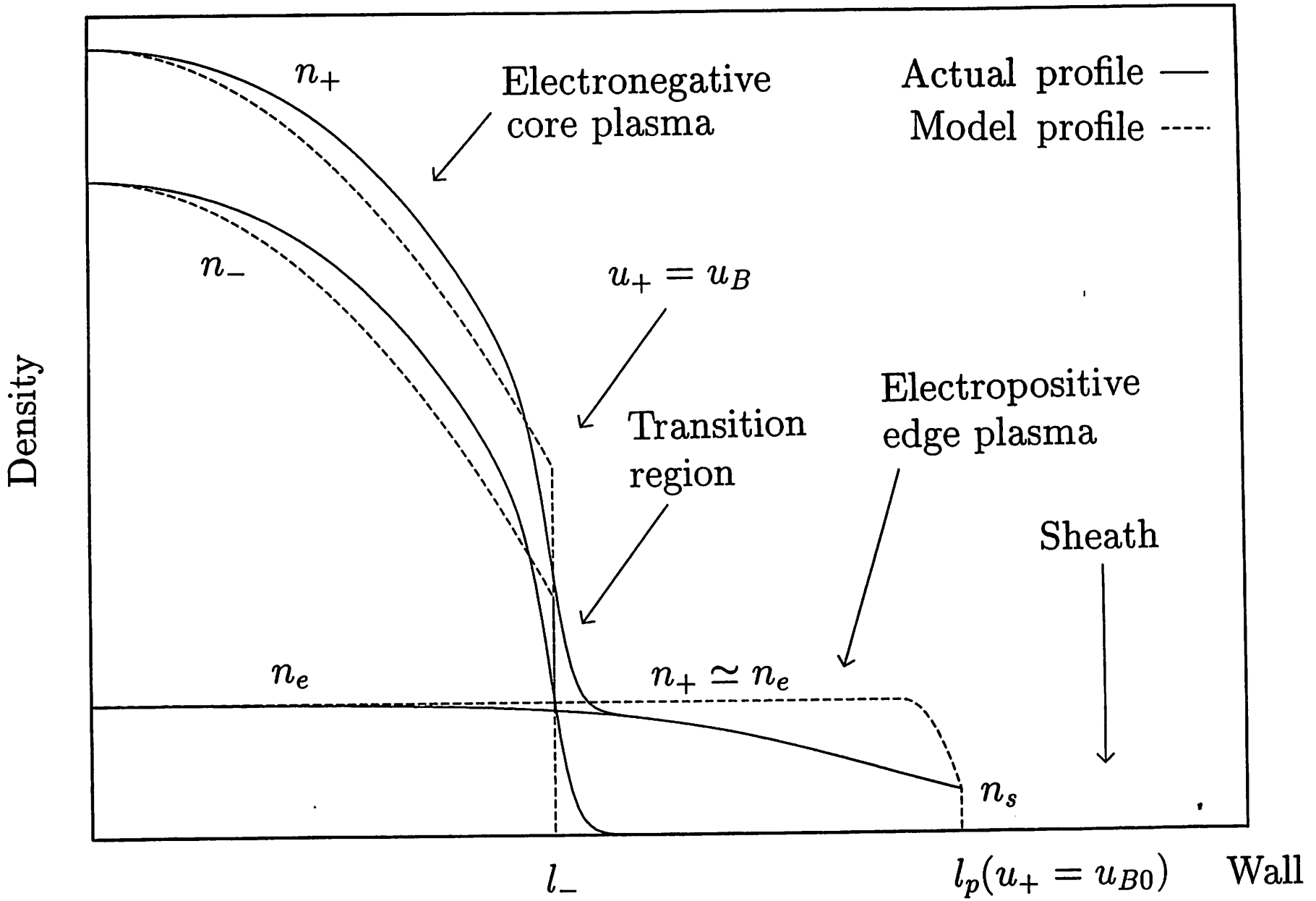
n_+
Electronegative
core plasma
Actual profile
Model profile
n_-
$u_+ = u_B$
Density
Transition
region
Electropositive
edge plasma
Sheath
n_e
$n_+ \simeq n_e$
n_s
l_-
$l_p(u_+ = u_{B0})$
Wall

Fig. 2

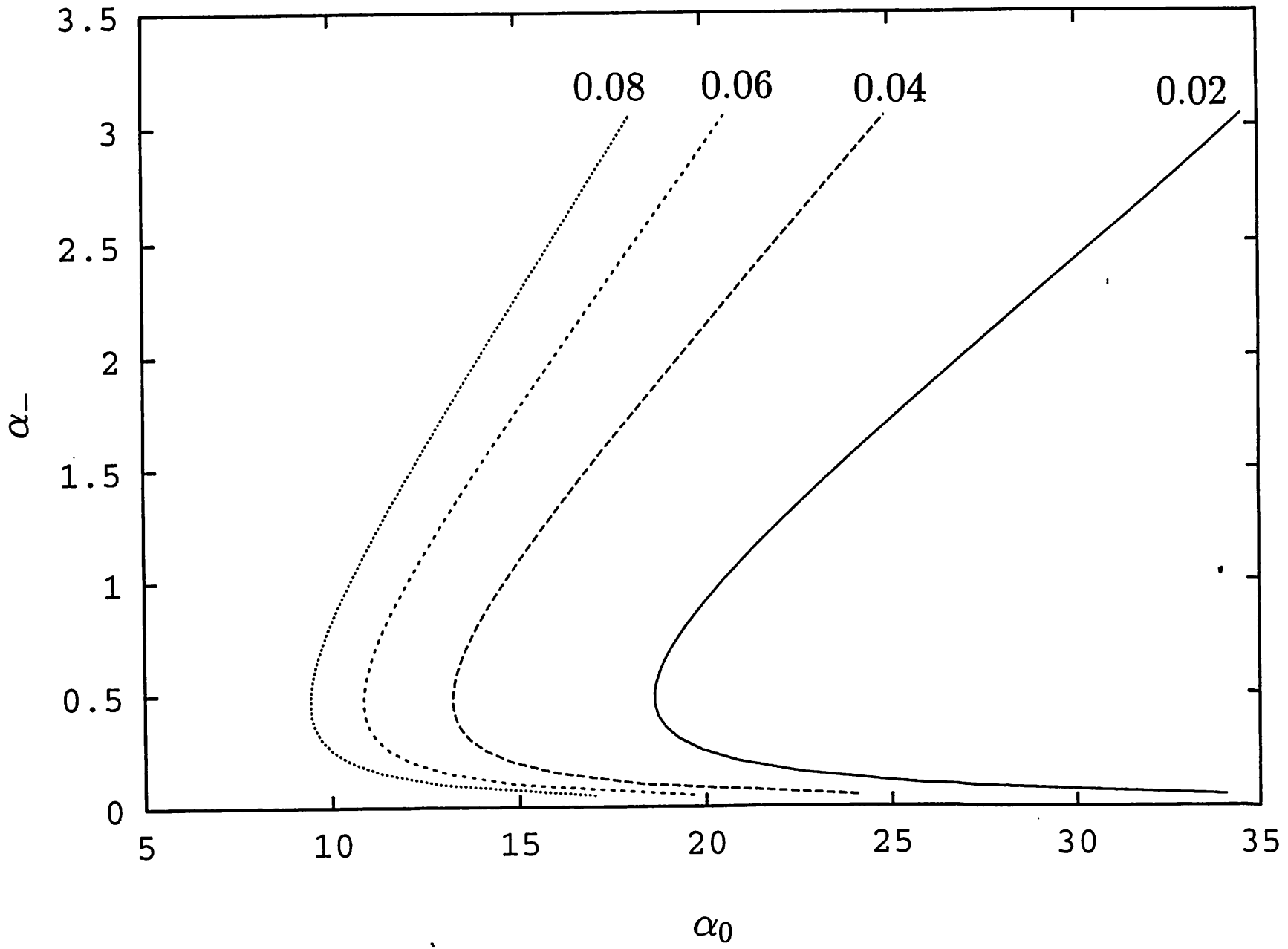

Fig. 3a

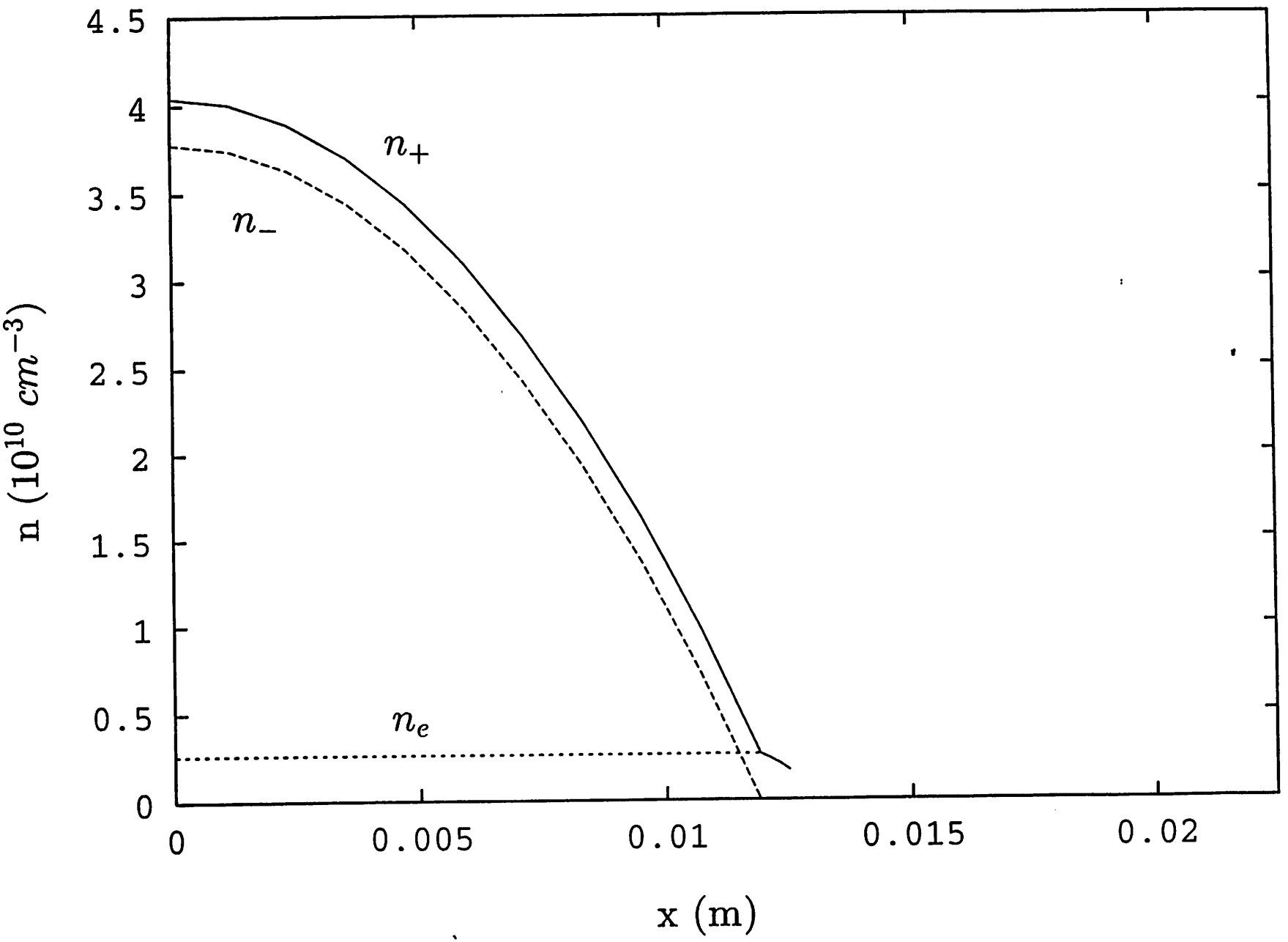

Fig. 3b

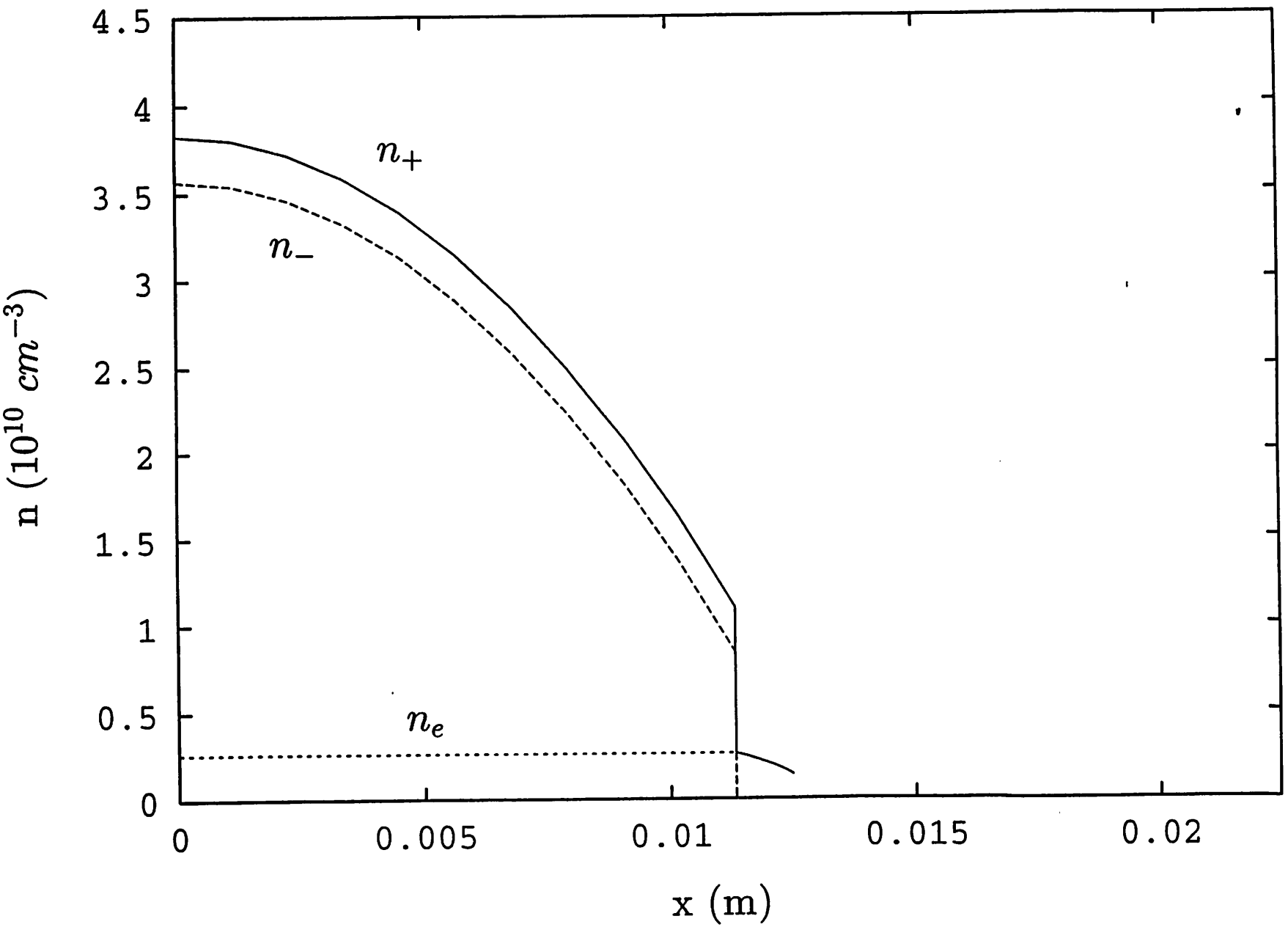

Fig. 4a

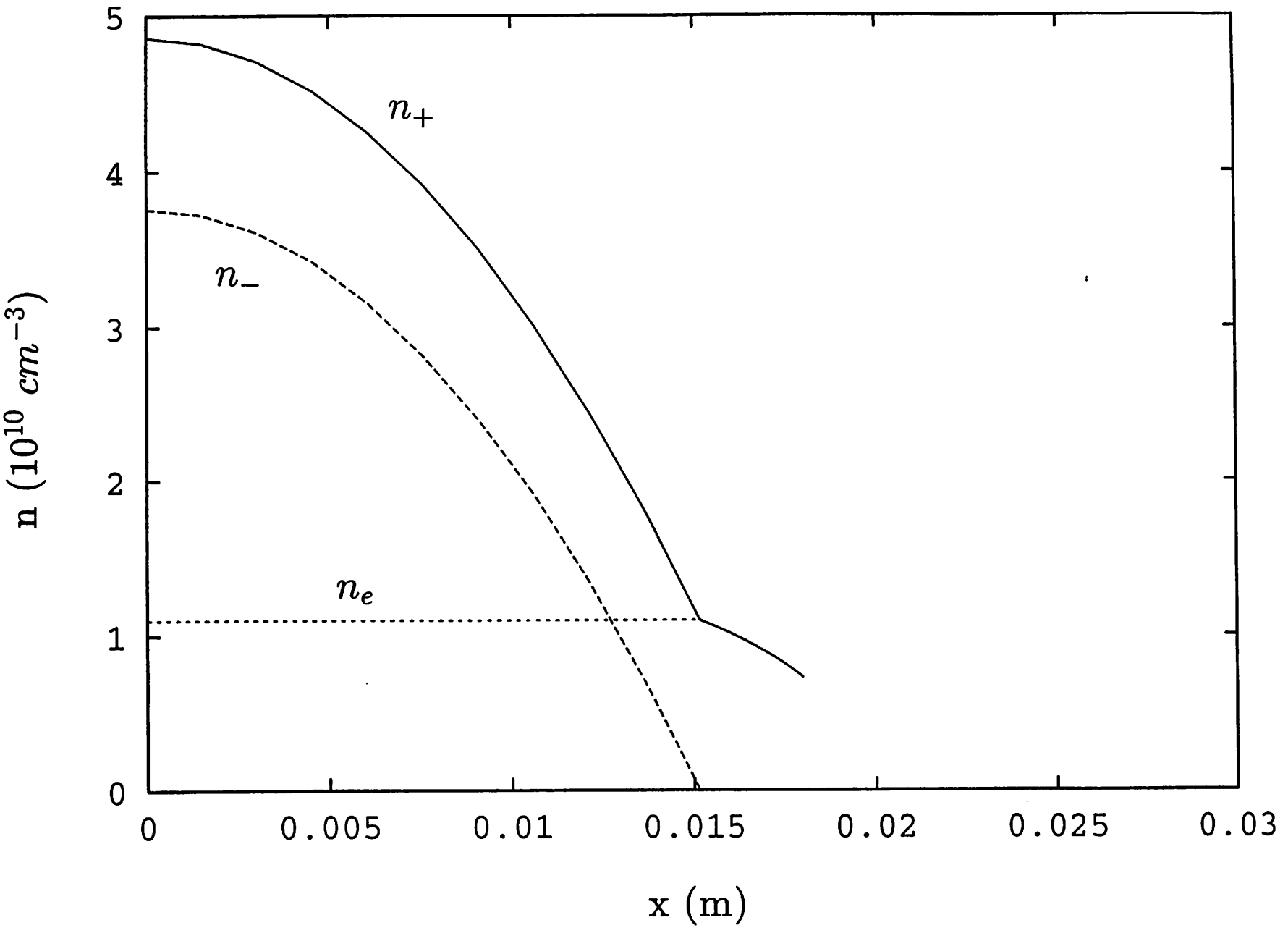

Fig. 4b

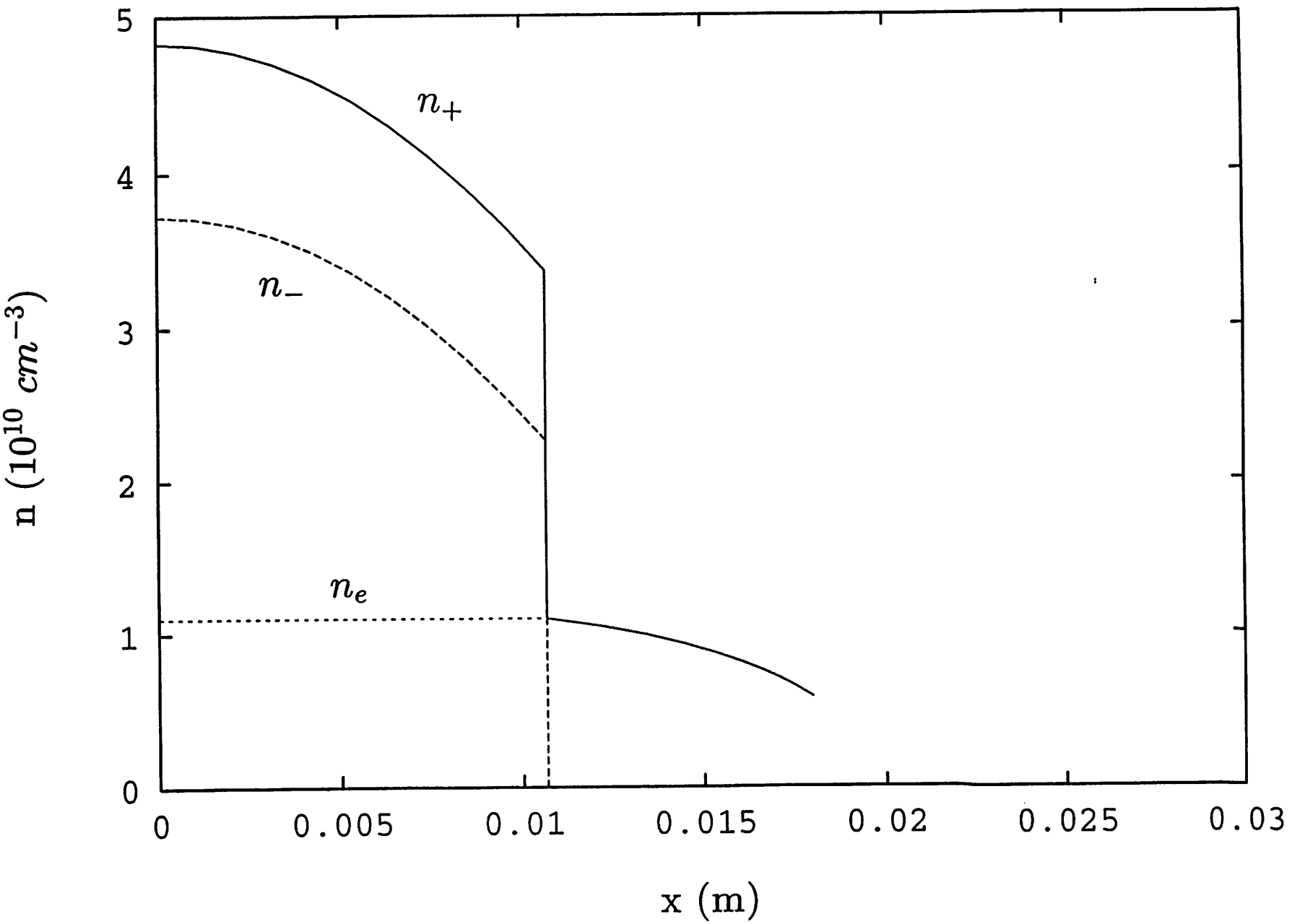

Fig. 5a

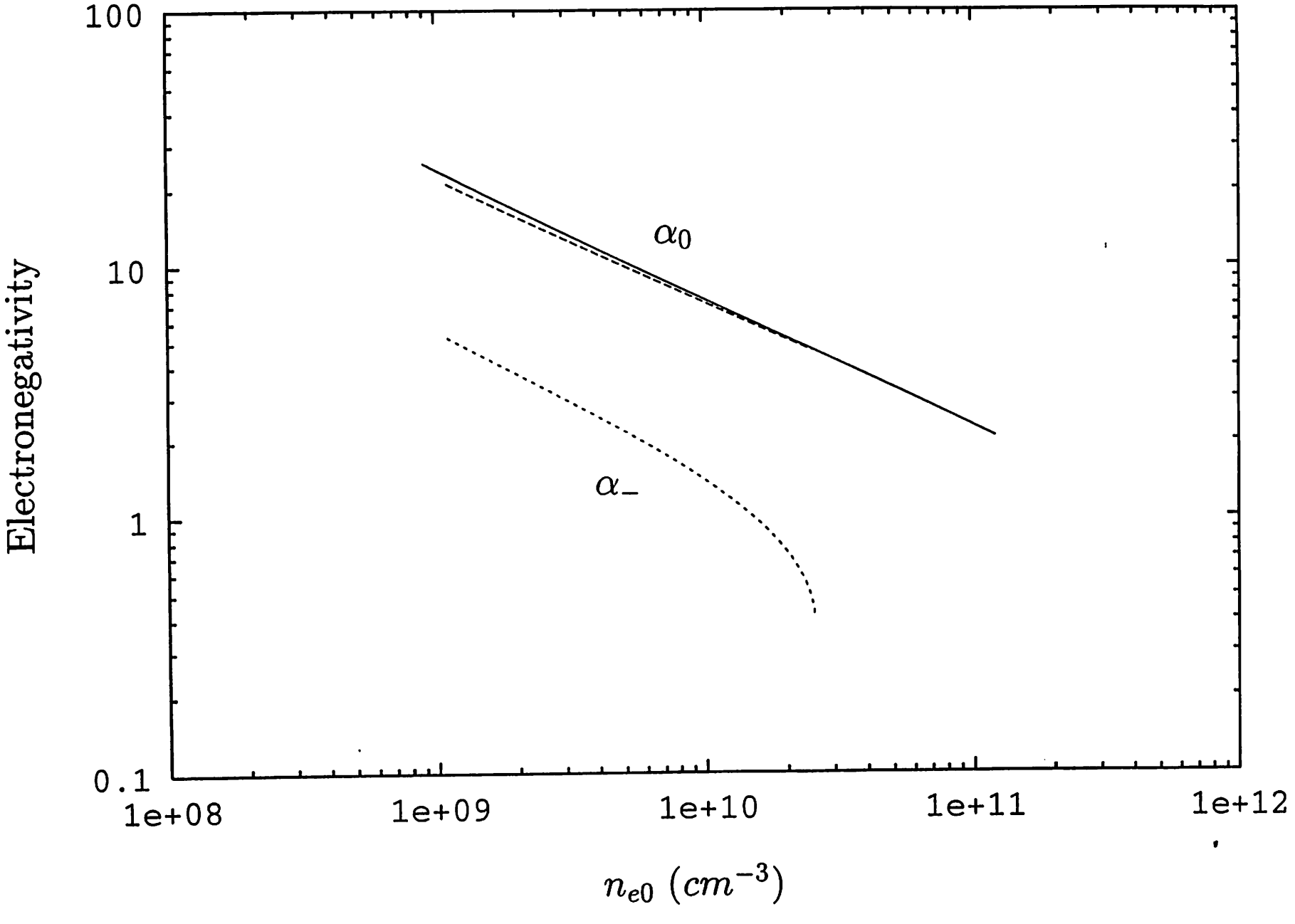
100
10
1
0.1
Electronegativity
α_0
α_-
1e+08
1e+09
1e+10
1e+11
1e+12
n_{e0} (cm^{-3})

Fig. 5b

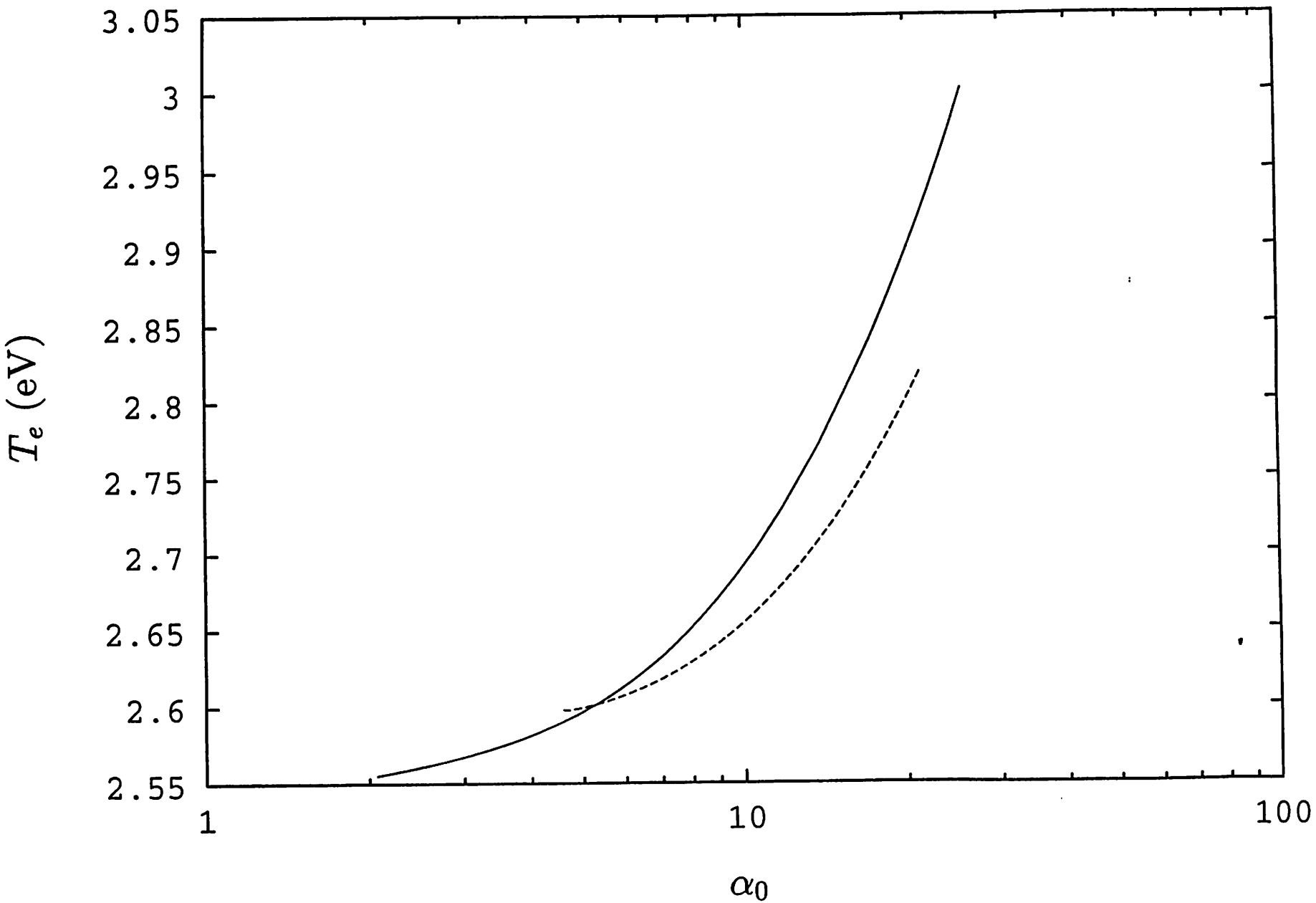

Fig. 5c

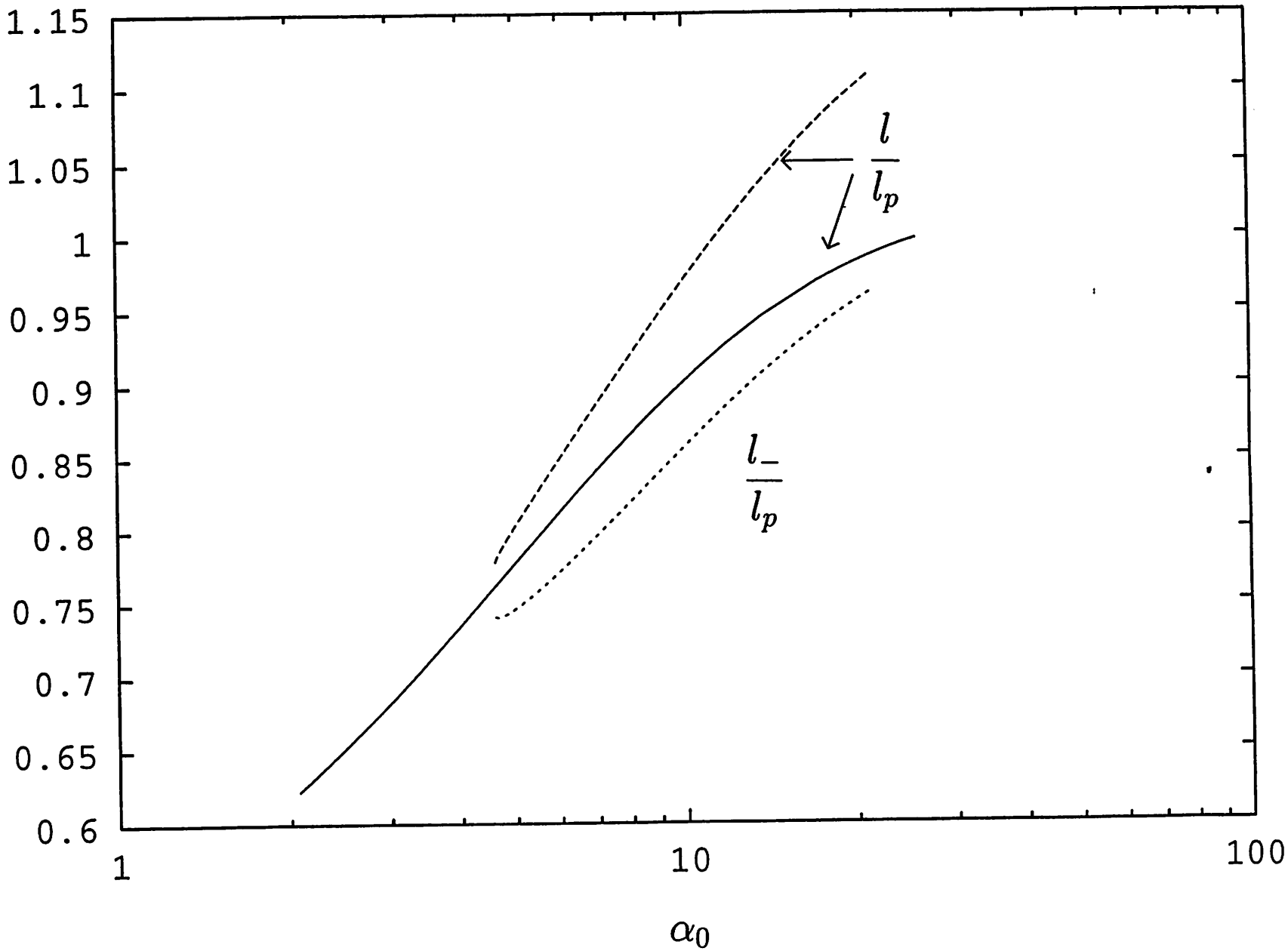
1.15
1.1
1.05
1
0.95
0.9
0.85
0.8
0.75
0.7
0.65
0.6
1
10
100
α_0
$\frac{l}{l_p}$
$\frac{l_-}{l_p}$

Fig. 6a

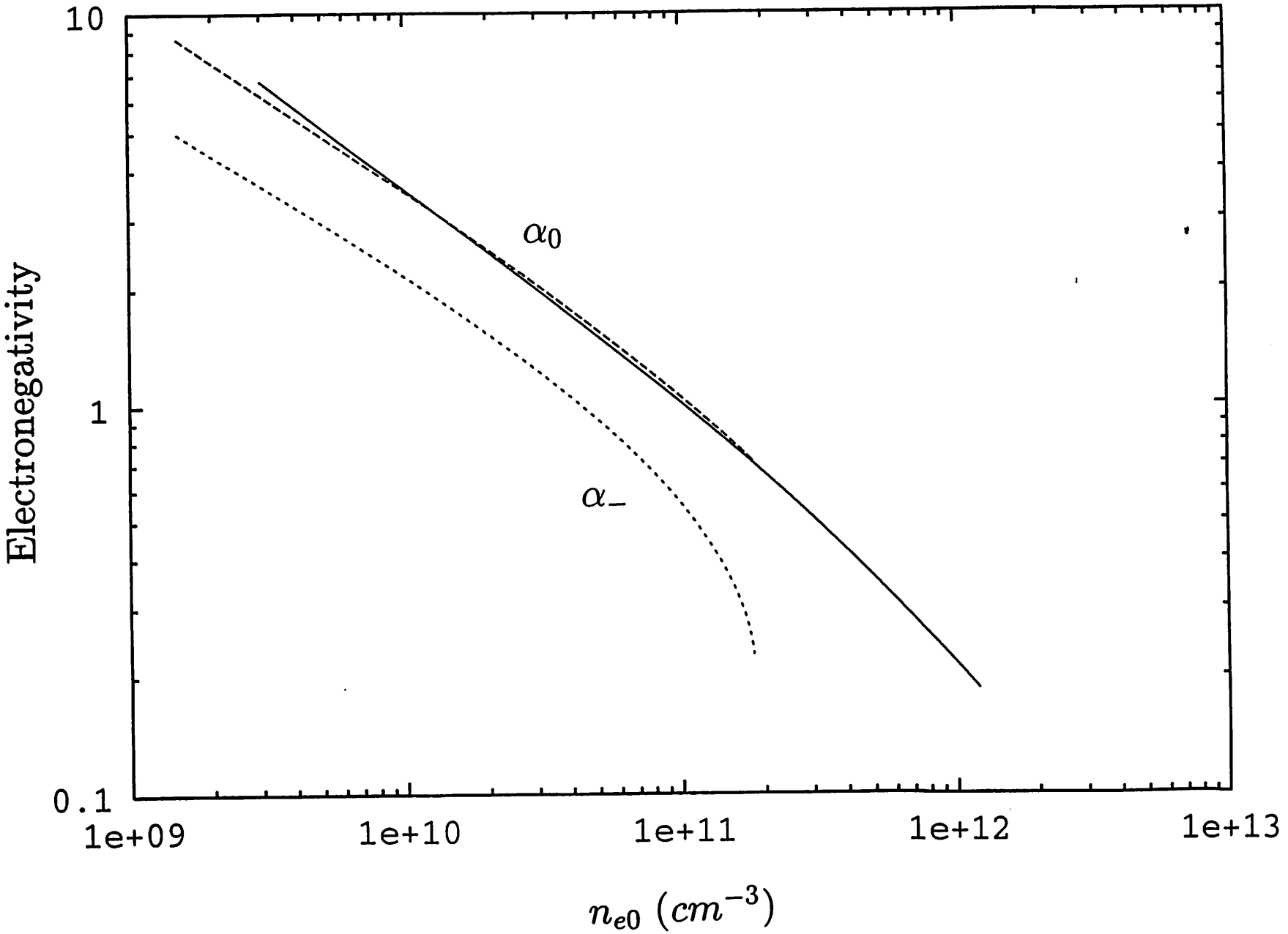
10
1
0.1
Electronegativity
α_0
α_-
1e+09
1e+10
1e+11
1e+12
1e+13
$n_{e0}\ (cm^{-3})$

Fig. 6b

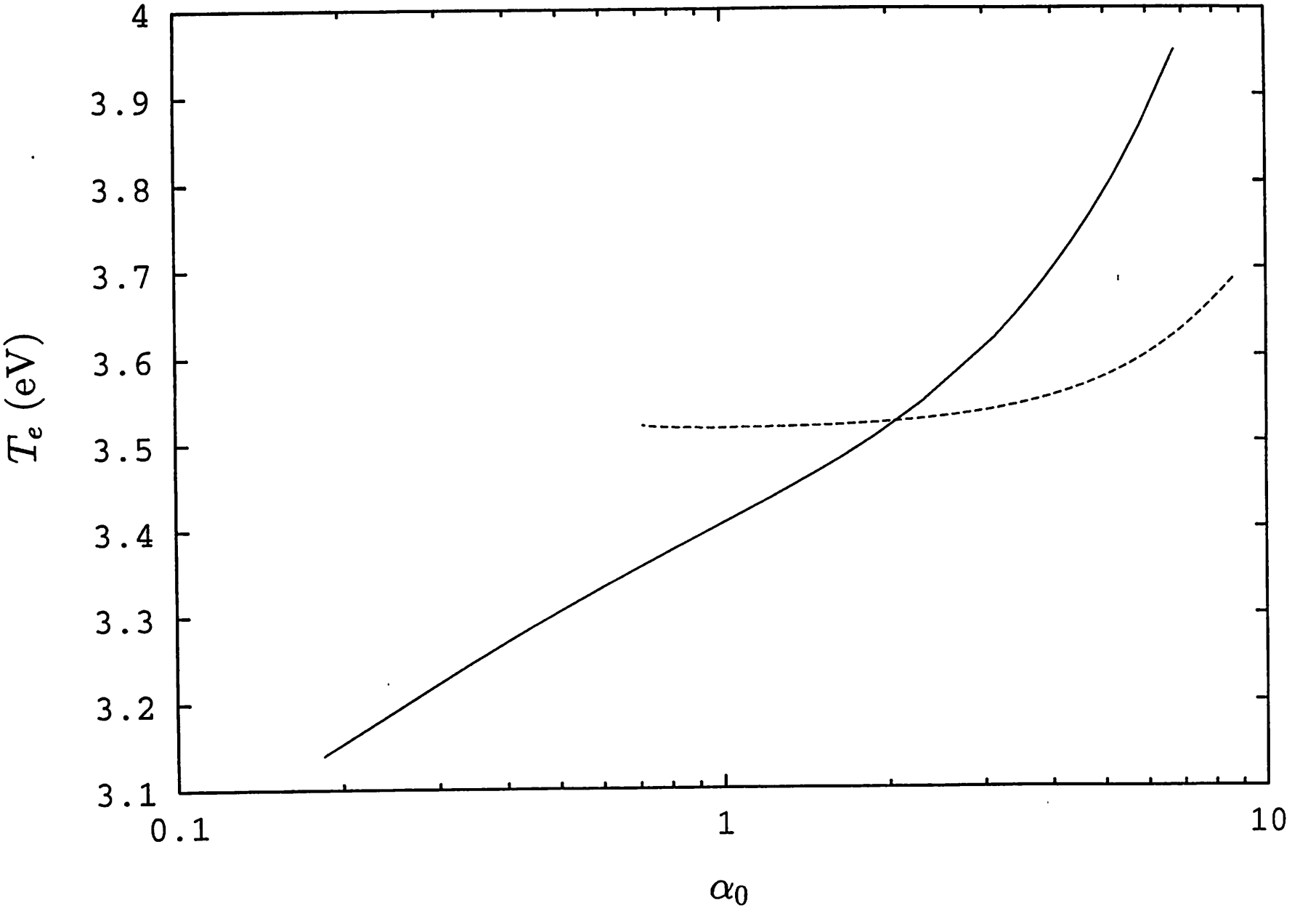

Fig. 6c

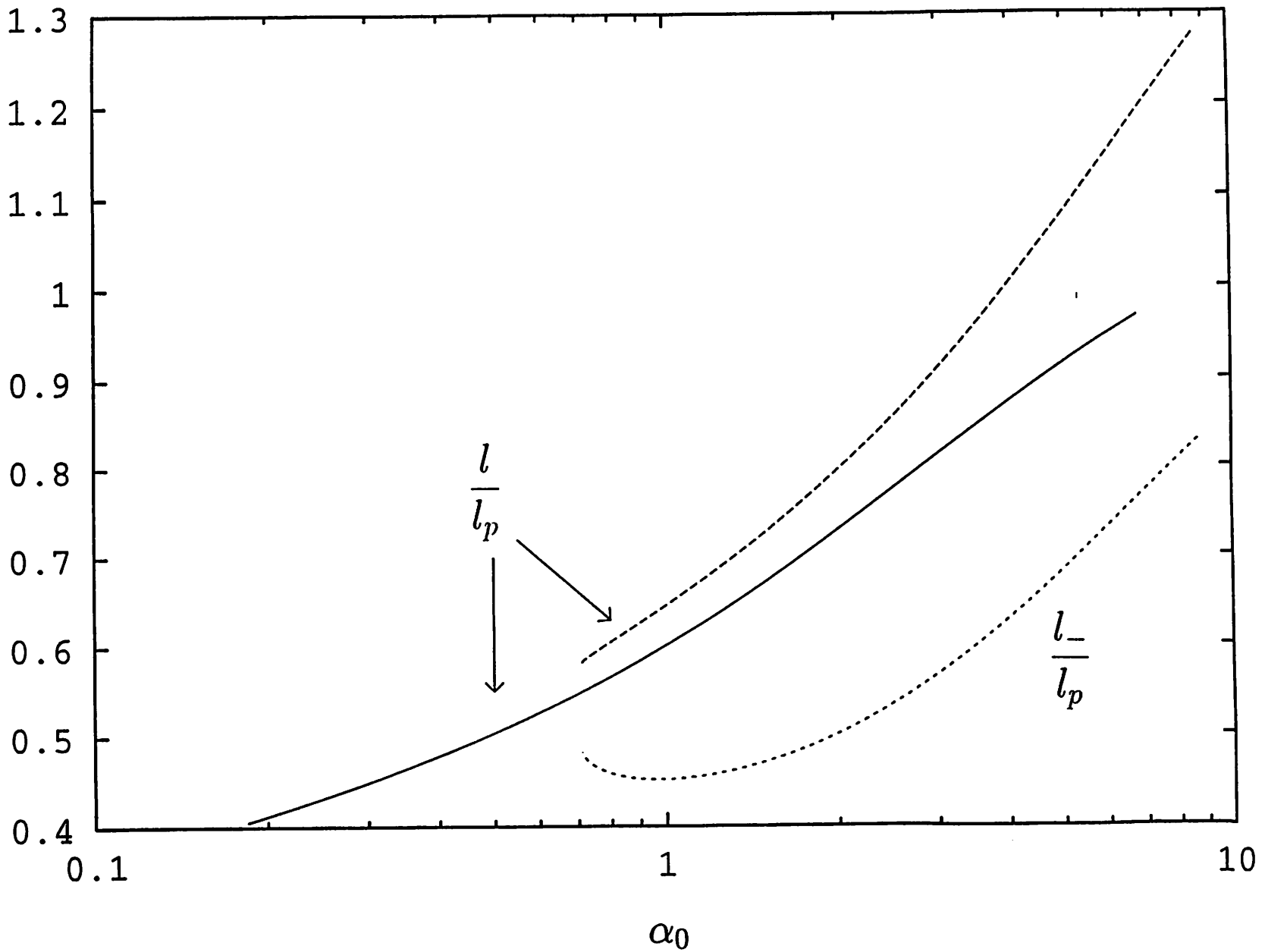

Fig. 7

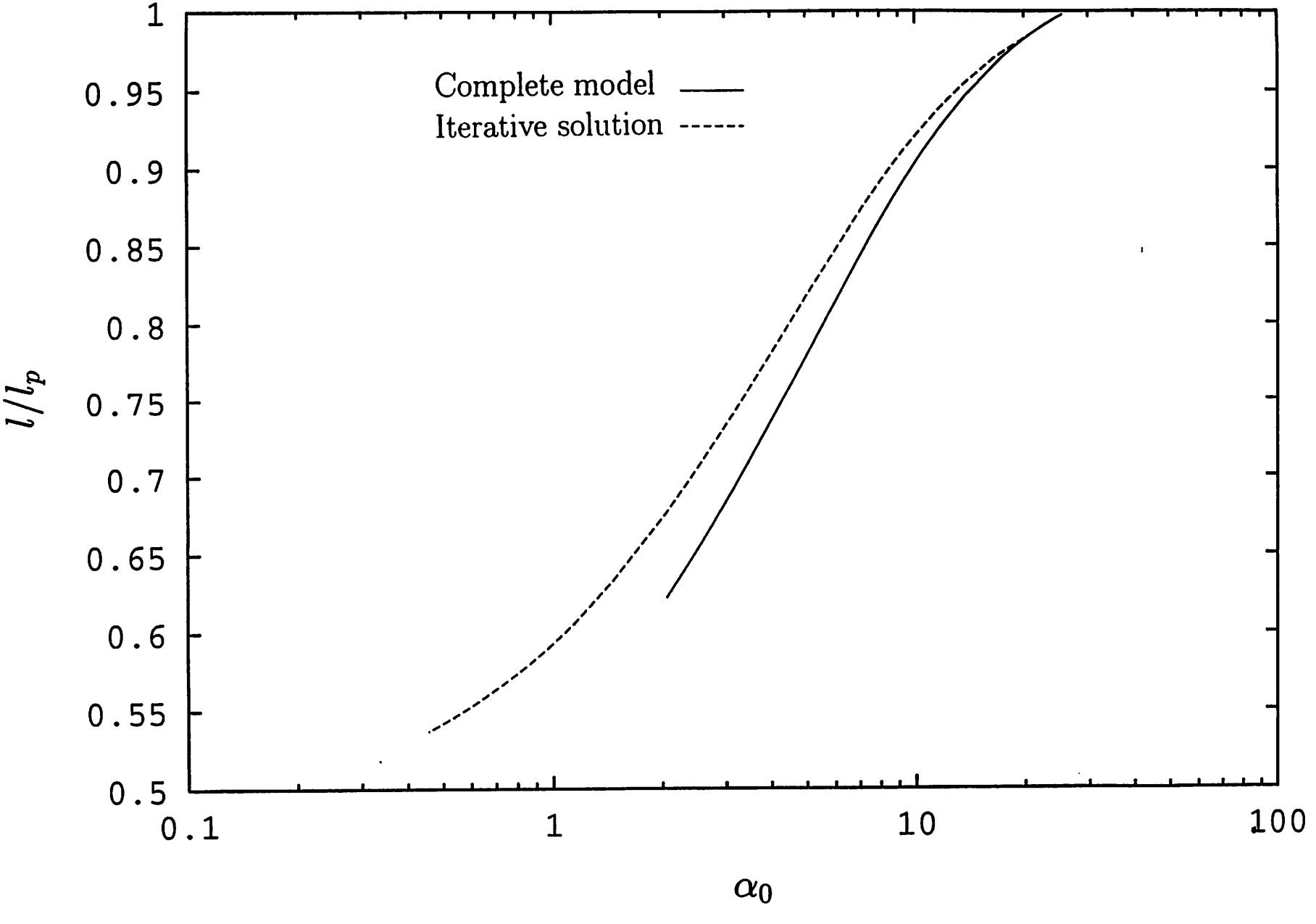
Complete model
Iterative solution
1
0.95
0.9
0.85
0.8
0.75
0.7
0.65
0.6
0.55
0.5
l/l_p
0.1
1
10
100
α_0

Fig. 8a

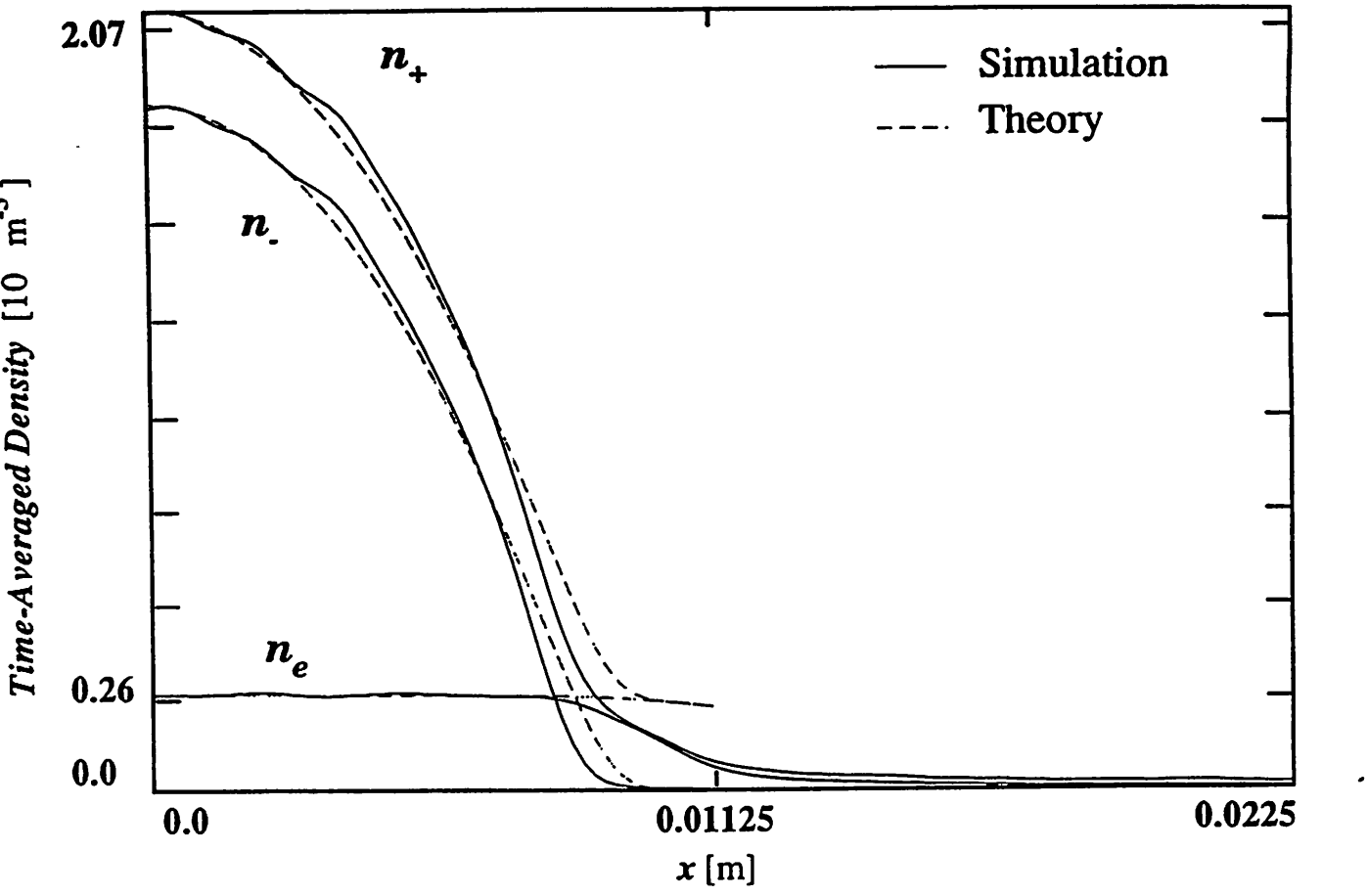
2.07
0.26
0.0
n_+
n_-
n_e
Simulation
Theory
Time-Averaged Density [10^{16} m^{-3}]
0.0
0.01125
0.0225
x [m]

Fig. 8b

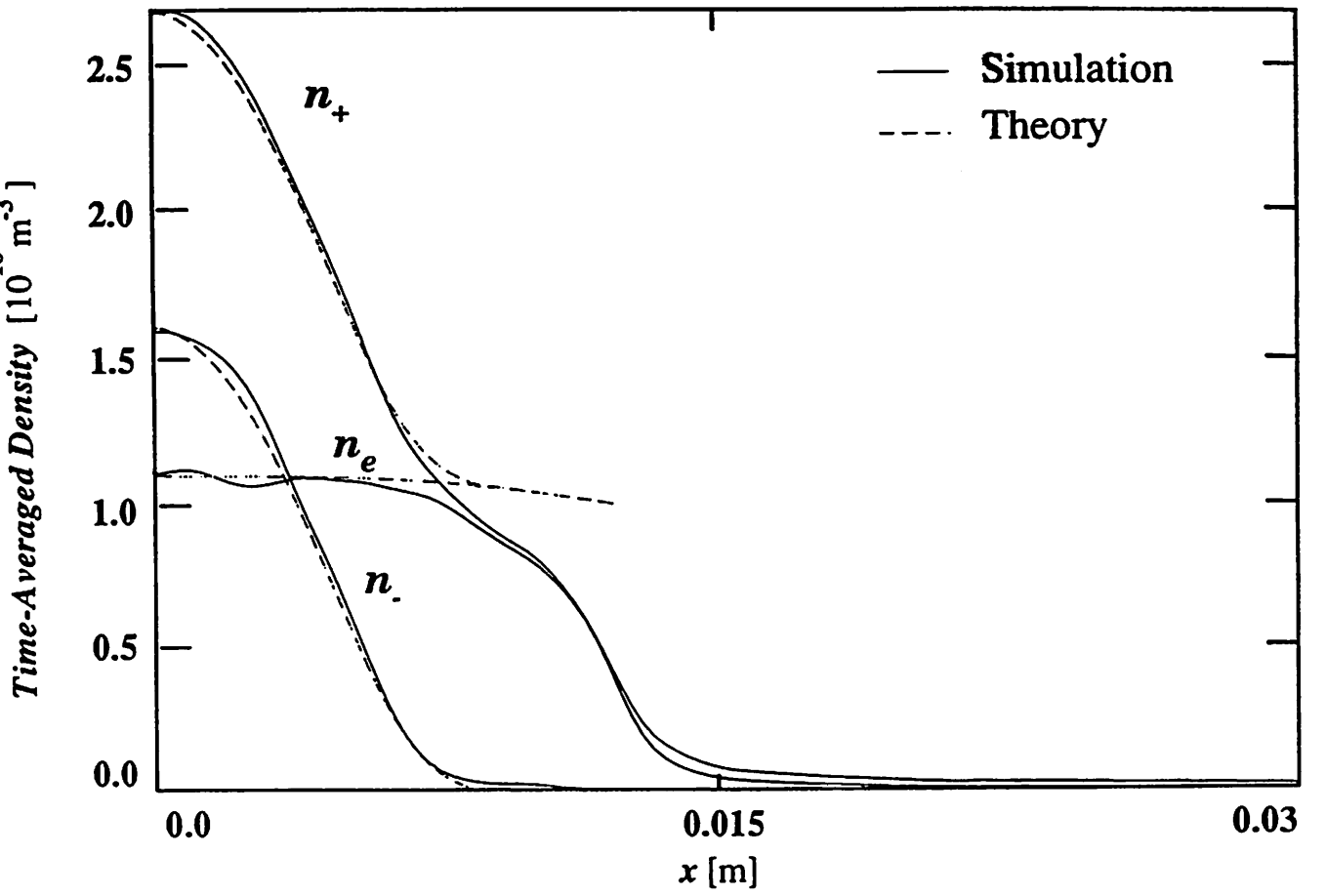
Simulation
Theory
n_+
n_e
n_-
2.5
2.0
1.5
1.0
0.5
0.0
0.0
0.015
0.03
x [m]
Time-Averaged Density [10^{16} m^{-3}]